NTNU
Norwegian University of
Science and Technology

Flavor Oscillations of High-Energy Neutrinos

Sergio Sánchez Navas

MSc in Physics
Submission date: May 2016
Supervisor: Michael Kachelriess, IFY

Norwegian University of Science and Technology
Department of Physics

NTNU

Flavor Oscillations of High-Energy Neutrinos

Sergio Sánchez Navas

Physics
Submssion date: May 15, 2016
Supervisor: Michael Kachelrieß

Norwegian University of Science and Technology
Department of Physics

Abstract

In this thesis, we study neutrino oscillations in vacuum and in the presence of a Dark Matter halo in the Milky Way. For that purpose, first describe the particle physics of neutrinos through an historical introduction. Then we focus on the Quantum Field Theory describing neutrinos in the Standard Model, weak interactions and electroweak unfication. We also discuss the methods and techniques of neutrino astronomy before finally making use of the data collected by IceCube and our numerical simulations to analyse high-energy neutrino oscillations. We conclude that relevant information about the cosmic sources could be extracted from the track-to-shower ratio of events when more precise statistics can be derived after more years of observation. We also consider the effects of Dark Matter on the oscillation probabilities and find that the mixing angle and the neutrino energy are the most relevant parameters.

Acknowledgements

First and foremost, I would like to express my gratitude to my supervisor, Prof. Michael Kachelrieß, for his guidance and help during the development of this work, providing not only up-to-date relevant sources but also precious advice in terms of layout and content.

I would also like to thank my good friends in Leserom B3-136 in Trondheim and Biblioteca María Zambrano in Madrid for a great working enviromnment and invaluable personal contributions thoughout these years.

Last but not least, I would like to thank my supporting parents for showing me the path to who I am now and for believing in me under any circumstances.

This work is dedicated to my aunt, uncle and cousins for inspiring discussions about science and beyond and specially to my beloved grandmothers for their kindness and love.

...a mi abuelo Miguel...

Contents

Chapter 1

Introduction

The purpose of this Master Thesis is to describe neutrino oscillations in the context of *High Energy Starting Events* (HESE) as detected by IceCube in Antarctica. Neutrino oscillation is an experimentally observed process included in what is called physics beyond the Standard Model (SM), whose study was motivated by two major problems: the atmospheric neutrino problem and the solar neutrino problem. The Nobel Prize in Physics 2015 was awarded to Takaaki Kajita from the Super-Kamiokande Collaboration, University of Tokyo, Japan, and Arthur B. McDonald from the Sudbury Neutrino Observatory Collaboration, Queens University, Kingston, Canada, "for the discovery of neutrino oscillations, which shows that neutrinos have mass" [1].

The body of this work is divided into four chapters, where we provide different approaches to neutrino physics. First of all, we cover the historical perspective of the discovery of the neutrino as an elementary particle, its peculiar nature and its three flavors as well as the need for neutrino oscillations to explain the observations of the second half of the 20th century. We then focus on the mathematical description of neutrinos as part of a Quantum Field Theory in the search for an explanation to their masses. Later, we dedicate a chapter to neutrino astronomy, including plausible sources for high-energy neutrinos and an overview on the detection methods with special attention to the IceCube detector as the state-of-the-art source of high-energy neutrino data. In the last chapter of this thesis we present our approach to two different applications of neutrino oscillations: the study of vacuum oscillations to obtain infomation about the sources and the study of oscillations in matter in the specific case of a Dark Matter halo (DM) in the Milky Way.

Throughout this work we will use the Lorentz-Heaviside convention of units $\hbar = c = \epsilon_0 = 1$ for derivations and calculations, if not stated otherwise.

Chapter 2

About neutrinos

In this Chapter we will introduce the neutrally charged particles called *neutrinos* in their historical context of discovery in order to justify the main purpose of this work, *neutrino oscillations*. We will then describe this process first in vacuum and then in presence of matter referring to experimental evidences to support the conclusions. The main source for the two firs Sections is David Griffith's textbook on particle physics [2] that we recommend reading for more details and anecdotes.

2.1 Early history and motivations

The story of the neutrino goes back to 1930 and the nuclear beta decay problem, where a radioactive nucleus splits into a lighter nucleus and an electron. In the center-of-mass frame the kinetical energies of this two-body decay are fixed and the outgoing particles appear *back-to-back*. However, experiments showed that the energy of the emitted electron was variable, challenging the conservation of energy law. Pauli proposed that a neutrally charged particle was carrying away the missing energy, leaving no track in a cloud chamber. He proposed to call it *neutron* [3]. Unfortunately there was little support for this theory and was mainly ignored, specially after Chadwick used that name in 1932 for his heavy neutral nucleon [4]. Later on, Fermi presented an accurate model for the β-decay of a neutron that included Pauli's idea as well as Dirac's concept of the *positron*, also suggesting this new particle to be extremely light, therefore calling it *neutrino* [5]. This decay would be then described by the reaction

$$n \to p^+ + e^- + \nu. \tag{2.1.1}$$

The kinematical argument for the two-body decay was also used by Powell in 1947 in the pion decay model. He published a picture in which a pion is seen to decay into a muon, that emerges with a 90° angle [6]. This clearly indicates that another particle must have emerged at the same time in the opposite direction. This particle has to be neutrally charged in order to leave no track on the cloud chamber, and the neutrino was again suggested,

$$\pi^- \to \mu^- + \nu. \tag{2.1.2}$$

A second picture was published by the same group that showed the decay of the latter muon into an electron, again with 90° (Fig. 2.1). This time it was suggested that the neutral missing item was actually two neutrinos instead of one, since the energy of the muon after the pion decay was fixed by experiments but the energy of the last electron

was varying [7]. This meaning that the final state consisted of at least three bodies, two of them neutral and lighter,

$$\mu^- \to e^- + 2\nu. \tag{2.1.3}$$

However, it was not until the mid-1950s that any exerimental evidence was found to justify these theories.

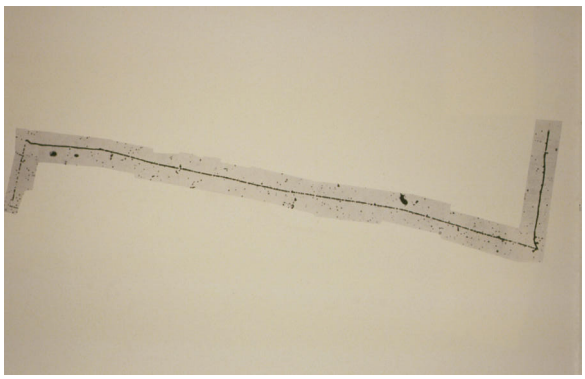

Figure 2.1: Pion decay into muon and neutrino. The muon then decays into an electron and two neutrinos [7].

2.2 Detection and aditional problems

Neutrinos rarely interact with matter and therefore an intense source is needed. Cowan and Reines studied the β-decay at the Savannah River nuclear reactor in the US. They thought that neutrinos would interact with protons to give neutrons and positrons, so they focused on detecting the number of positrons per hour to check with the predicted number of interactions from their initial flux. Their results gave experimental evidence to the existence of neutrinos [8],

$$p^+ + \nu \to n + e^+. \tag{2.2.1}$$

Since this new particle is neutrally charged, there was a big debate on whether it was its own antiparticle, like the neutral pion and the photon, or on the other hand it was not, like the antineutron. Following special relativity arguments, the crossed reaction also must happen,

$$n + \nu \to p^+ + e^-. \tag{2.2.2}$$

Therefore the question was if the same reaction could happen using antineutrinos,

$$n + \bar{\nu} \to p^+ + e^-. \tag{2.2.3}$$

This reaction was not found so Davis and Harmer determined that the neutrino and the antineutrino are indeed different particles [9].

In 1953, Konopinski and Mahmoud proposed the law of conservation of *lepton number*, where the sum of the lepton number on both sides of a reaction had to agree [10]. They assigned the value $L = +1$ to the electron, the muon and the neutrino, while a value $L = -1$ was given to the positron, the positive muon and the antineutrino. Following this reasoning, the neutron would only react with neutrinos to give protons and electrons.

Also according to this law, the β-decay and the inverse β-beta decay should involve only antineutrinos and thus be written as

$$\begin{aligned} n &\rightarrow p^+ + e^- + \bar{\nu}, \\ p^+ + \bar{\nu} &\rightarrow n + e^+, \end{aligned} \tag{2.2.4}$$

the charged pion decays as

$$\begin{aligned} \pi^- &\rightarrow \mu^- + \bar{\nu}, \\ \pi^+ &\rightarrow \mu^+ + \nu, \end{aligned} \tag{2.2.5}$$

and the muon decays as

$$\begin{aligned} \mu^- &\rightarrow e^- + \nu + \bar{\nu}, \\ \mu^+ &\rightarrow e^+ + \nu + \bar{\nu}. \end{aligned} \tag{2.2.6}$$

However, it has never been observed an event in which a muon decayed into an electron plus a photon, even though the lepton number is conserved. This means that another conservation law must be preventing it,

$$\mu^- \nrightarrow e^- + \gamma. \tag{2.2.7}$$

The solution to this question was a conservation of lepton number for each *generation* and associating one type of neutrino to the muon and another to the electron. In order to verify this, a dedicated experiment was conducted at Brookhaven where they used muon antineutinos from the π^- decay to check if they reacted with protons to produce antimuons and neutrons[11]. If this rule was not correct, they expected to find also positrons as a result. The conclusion was that only muons were detected, confirming the two-family hypothesis,

$$\bar{\nu}_\mu + p^+ \rightarrow \mu^+ + n. \tag{2.2.8}$$

Therefore we have to adjust again the previous reactions to follow this new law,

$$\begin{aligned} n &\rightarrow p^+ + e^- + \bar{\nu}_e \\ \pi^- &\rightarrow \mu^- + \bar{\nu}_\mu \\ \pi^+ &\rightarrow \mu^+ + \nu_\mu \\ \mu^- &\rightarrow e^- + \nu_\mu + \bar{\nu}_e \\ \mu^+ &\rightarrow e^+ + \bar{\nu}_\mu + \nu_e. \end{aligned} \tag{2.2.9}$$

2.3 The third generation

"The letter τ is from Greek $\tau\rho\iota\tau o\nu$ for *third* - the third charged lepton."
-Martin L. Perl

Until the late 1960s, lepton physics remained calm. Many research groups focused their attention on finding a correlation between the electron and the muon [12], probing different paths such as special interactions with hadrons. This was not a fruitful field and some other directions were taken, like the existence of more types of charged leptons. In

this way, the *sequential lepton* theory was suggested by Perl and Rapidis in 1972 to refer to the hypothesis of pairs [13]

$$\begin{array}{ll} e^- & \nu_e \\ \mu^- & \nu_\mu \\ \mu'^- & \nu'_\mu \\ \mu''^- & \nu''_\mu \end{array} \tag{2.3.1}$$

with further terms meaning heavier leptons.

The search for these new particles was based on e^-e^+ annihilation at particle accelerators such as the SPEAR e^-e^+ storage ring in 1973. The design proposed for the Mark I detector followed the idea of the decay of the muon into electron plus neutrino and antineutrino [14]. High-energy pairs of electron and positron would annihilate and create pairs lepton-antilepton that would then decay into electrons, muons and the corresponding netrinos,

$$\begin{aligned} e^- + e^- &\rightarrow l^- + l^+ \\ l^- &\rightarrow e^- + \nu_l + \bar{\nu}_e \\ l^+ &\rightarrow \mu^+ + \nu_\mu + \bar{\nu}_l, \end{aligned} \tag{2.3.2}$$

and all other combined posibilities. The detector would then look for an excess in $e - \mu$ events with missing energy carried out by neutrinos.

The detector started working with an energy of 4.8 GeV with useful luminosity and a top energy of 8 GeV and by 1975 a relevant number of events involving an electron and a muon of oposite charges and no other charged particles or photons were detected. These events could not be explained with the existing methods and the heavy lepton solution became the main option [15]. It was proposed that a pair of new particles each from 1.6 to 2 GeV decayed into electrons, muons and missing neutrinos. Perl called this unknown particle U. The name τ was later suggested by P. Rapidis. Speculation began around the posibility of these events being a misinterpretation of the decay of the recently discovered *charmed* particles, as there were found excess of electron and muon events but the pion decay mode was still not found, setting an upper limit for the branching ratio with a lower value than the predicted by theory,

$$\tau^- \rightarrow \pi^- + \nu_\tau \tag{2.3.3}$$

Finally, during 1978, the branching ratio associated to this reaction was confirmed to be close to the expected 10% [12]. This confirmed also the existence of a third flavor of neutrinos.

2.4 Neutrino oscillations

Primary cosmic rays consist of high-energy charged particles that interact with the nucleus of oxygen and nitrogen atoms in the atmosphere. Protons collide with this nuclei and produce mainly pions, that will decay into muons and neutrinos as described in Eq. (2.2.9). These will also decay into electrons or positrons and neutrinos, so that

the expected atmospheric neutrino beam would consist of approximately twice as many muon-neutrinos as electron-neutrinos. These neutrinos can interact with the nuclei of heavy atoms in large detectors and produce muons or electrons, which can then be observed via the Cherenkov effect in water, as we will discuss in Chap. 4. However, the experimental data at Kamiokande [16] showed a deficit in muon-neutrinos, while the number electron-neutrinos agreed with expectations. The analysis of the systematic effect and the study of the experimental data suggested that the explanation was that the missing muon-neutrinos had *oscillated* into tau-neutrinos. This could only happen if neutrinos have nonzero mass, so that the three families are a mixed state in which the weak eigenstates $\nu_e,\ \nu_\mu$ and ν_τ are a superposition of three mass eigenstates $\nu_1,\ \nu_2$ and ν_3. Therefore, if the muon-neutrino produced in the pion decay was a mixture of two mass eigenstates, these would propagate with slightly different velocities so they would get out of phase and a different flavor could be detected. This could never happen if neutrinos were truly massless.

If we now assume two-flavor mixing, the weak and mass eigenstates can be related as

$$\begin{aligned} \nu_e &= \nu_1 \cos\theta + \nu_2 \sin\theta \\ \nu_\mu &= \nu_2 \cos\theta - \nu_1 \sin\theta, \end{aligned} \tag{2.4.1}$$

where θ is the mixing angle. The time dependence of these eigenstates is

$$\begin{aligned} \nu_1(t) &= \nu_1(0)\mathrm{e}^{-iE_1 t} \\ \nu_2(t) &= \nu_2(0)\mathrm{e}^{-iE_2 t}. \end{aligned} \tag{2.4.2}$$

Inserting this dependence in the previous equations we can find the probability that an electron-neutrino oscillates into a muon-neutrino as

$$P_{\nu_e \to \nu_\mu} = \left[\sin(2\theta) \sin\left(\frac{E_2 - E_1}{2} t \right) \right]^2 \tag{2.4.3}$$

or in terms of distance traveled $z \approx ct$ and mass differences

$$P_{\nu_e \to \nu_\mu} = \left\{ \sin(2\theta) \sin\left[\frac{(m_2^2 - m_1^2)}{4E} z \right] \right\}^2. \tag{2.4.4}$$

In this way we can define an oscillation distance as

$$L = \frac{2\pi E}{(m_2^2 - m_1^2)}, \tag{2.4.5}$$

where the oscillation probability is maximum.

Observations from Kamiokande and SuperKamiokande [17] proved this hypothesis and provided a mixing angle and a mass difference

$$\theta_{\mathrm{atm}} \approx \pi/4, \qquad \Delta(m)^2_{\mathrm{atm}} \approx 3 \times 10^{-3}\mathrm{eV}^2. \tag{2.4.6}$$

Another relevant scenario that helped greatly to accept the theory of neutrino oscillations was the resolution to the Solar neutrino problem, which was awarded a Nobel Prize in 2015. In 1938, Hans Bethe proposed that the Sun is indeed a nuclear fusion

reactor and that the radiation we receive from it comes primarily from hydrogen burned to helium. This explained both the luminosity and the longevity of the Sun better than previous theories based on gravity or fission as sources of radiation. In this process, called *proton-proton chain*, protons in the solar core combine to produce helium nuclei, or *alpha*-particles, in a series of reactions involving fusion, that emit photons, and β-decays, that emit neutrinos in the range 0.1-10 MeV. 86% of solar neutrinos are produced in the first step, where two protons form a deuteron neucleus and emit a positron and a neutrino. 14% are emitted when ^{7}Be decays into ^{7}Li capturing an electron. Finally, the most energetic 0.02% are emitted when ^{8}B decays into ^{8}Be plus positron plus neutrino. This reactions produce only electron-neutrinos, so the Sun is a pure source of this flavor. In 1968, Ray Davis *et al.* [18] detected the first flux of solar neutrinos at the Homestake mine, as we will describe in Sec. 4.3. However, they reported a deviation of about 70% from the expected number of events based on their model. Other experiments such as Kamiokande and SuperKamiokande [19] also reported similar deviations from the predicted flux.

In 1957, Bruno Pontecorvo suggested that neutrinos could oscillate, as an analogy to the $K^0/\bar{K}^0$ oscillations [20]. He later recovered this idea and proposed that those neutrinos might have changed into another flavor or into antineutrinos, so that the experiment designed specifically to detect electron-neutrinos was blind to them [21]. The Super-Kamiokande experiment was designed using water as detector, so that Cherenkov radiation could be observed in every elastic neutrino-electron scattering event. This method is sensitive to all neutrino flavors, although the actual flavor of the incoming neutrino could not be determined and the detector efficiency was 6.5 times larger for electron-neutrinos than for the other two. In 2001 they reported the detection of 45% of the predicted flux.

A similar experiment was carried out at the Sudbury Neutrino Observatory (SNO) using heavy water, which is sensitive to the elastic scattering process and other two reactions,

$$\nu + e \rightarrow \nu + e \tag{2.4.7}$$
$$\nu + d \rightarrow n + p + \nu \tag{2.4.8}$$
$$\nu_e + d \rightarrow p + p + e. \tag{2.4.9}$$

In the summer of 2001, the SNO collaboration reported the detection of 35% of the predicted electron-neutrino flux, so that the 10% extra detected at SuperKamiokande could be due to muon- or tau-neutrinos [22]. In April 2002 they presented the measurements of both the total neutrino flux and the electron-neutrino flux [23], confirming the oscillation hypothesis (and therefore that neutrinos have mass) and provided the mixing angle and the square mass difference for the electron-neutrinos changing into the other flavors as

$$\theta_{sol} \approx \pi/6, \qquad \Delta(m^2)_{sol} \approx 8 \times 10^{-5}\text{eV}^2. \tag{2.4.10}$$

Equation (2.4.10) suggests that one mass splitting is rather small, while equation (2.4.6) indicates that another mass splitting is much larger. The third mass difference is then dependent on the other two. If we consider ν_3 as the heaviest, we can construct the *normal* neutrino mass hierarchy. However, it can be that the structure is the opposite and we get the *inverted* hierarchy where ν_3 is the lightest, as shown in Fig.2.2.

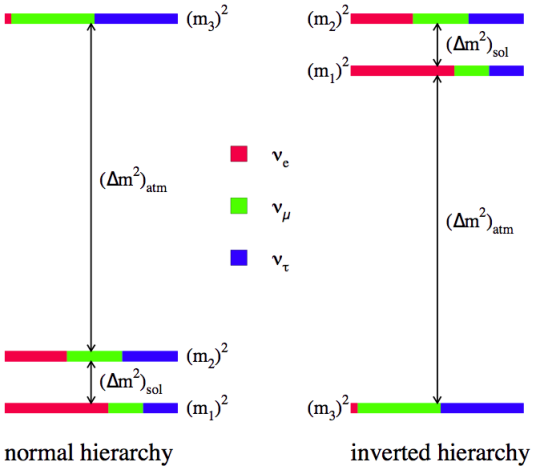

Figure 2.2: Normal and inverted neutrino mass hierarchies. The colours represent the estimated flavor composition in each mass eigenstate. Credit: [24]

Neutrino oscillations are thus a quantum mechanical consequence of the existence of non-zero neutrino masses, neutrino mixing and of the relatively small splitting between the neutrino masses. We can view the flavor and mass eigenstates of the neutrinos as the components of two vector and then rewrite Eq. (2.4.1) using a mixing matrix, that must be unitary. For the three neutrino flavors we have

$$\begin{pmatrix} \nu_e \\ \nu_\mu \\ \nu_\tau \end{pmatrix} = U_{3\times 3} \begin{pmatrix} \nu_1 \\ \nu_2 \\ \nu_3 \end{pmatrix}, \tag{2.4.11}$$

In the two-flavor oscillation frame, U has one nontrivial free parameter, the mixing angle θ. For three [resp. n] families, the mixing matrix would have three [resp. $\frac{1}{2}n(n-1)$] nontrivial angles θ_j . In addition, for Dirac neutrinos it has one [resp. $\frac{1}{2}(n-2)(n-1)$] Charge-Parity(CP)-violating phase(s), and three [resp. $\frac{1}{2}n(n-1)$] nontrivial phases for Majorana neutrinos. However, only the number of phases given by the Dirac case can be measured via neutrino oscillation experiments. We find the Maki-Nakagawa-Sakata (MNS) matrix for three flavors as

$$U_{3\times 3} = \begin{pmatrix} c_{12}c_{13} & s_{12}c_{13} & s_{13}e^{-i\delta} \\ -s_{12}c_{23} - c_{12}s_{23}s_{13}e^{i\delta} & c_{12}c_{23} - s_{12}s_{23}s_{13}e^{i\delta} & s_{23}c_{13} \\ s_{12}c_{23} - c_{12}s_{23}s_{13}e^{i\delta} & -c_{12}c_{23} - s_{12}s_{23}s_{13}e^{i\delta} & c_{23}c_{13} \end{pmatrix} \times \begin{pmatrix} 1 & 0 & 0 \\ 0 & e^{i\alpha_1/2} & 0 \\ 0 & 0 & e^{i\alpha_2/2} \end{pmatrix}, \tag{2.4.12}$$

where $c_{ij} \equiv \cos\theta_{ij}$, $s_{ij} \equiv \sin\theta_{ij}$, δ is the CP-violating phase and α_1, α_2 are the Majorana phases. This matrix is often called PMNS-matrix, to credit Pontecorvo for his original suggestion of neutrino oscillations.

Experimentally, we cannot measure directly the values of the mixing angles and the CP-phase, only the squared value of the sines and cosines of the angles. A global fit using present data was made by Gonzalez-Garcia *et al.* [25] and it is shown in Table 2.1. These values are inconsistent with tribimaximal neutrino mixing ($\theta_{12} = \theta_{23} = 45°$ and $\theta_{13} = 0°$). This analysis also disfavours $\theta_{13} = 0$ and θ_{23} equal to exactly 45 degrees, which would imply maximal mixing between the second and third neutrino mass eigenstates. It is interesting to mention that θ_{23} is the only PMNS matrix parameter which is strongly

Table 2.1: Three-flavor oscillation parameters after the Neutrino 2012 conference [25]. The lower range of θ_{23} is favoured for the normal mass hierarchy, while the higher range is for inverted hierarchy.

	best fit $\pm 1\sigma$	3σ range
$\sin^2\theta_{12}$	$0.302^{+0.013}_{-0.012}$	$0.267 \to 0.344$
$\theta_{12}(^\circ)$	$33.36^{+0.81}_{-0.78}$	$31.09 \to 35.89$
$\sin^2\theta_{23}$	$0.413^{+0.037}_{-0.025} \oplus 0.594^{+0.021}_{-0.022}$	$0.342 \to 0.667$
$\theta_{13}(^\circ)$	$40.0^{+2.1}_{-1.5} \oplus 50.4^{+1.3}_{-1.3}$	$31.09 \to 35.89$
$\sin^2\theta_{13}$	$0.0227^{+0.0023}_{-0.0024}$	$0.0156 \to 0.0299$
$\theta_{13}(^\circ)$	$8.66^{+0.44}_{-0.46}$	$7.19 \to 9.96$
$\delta_{CP}(^\circ)$	300^{+66}_{138}	$0 \to 360$
$\Delta m^2_{21}(\times 10^{-5}\mathrm{eV}^2)$	$7.50^{+0.18}_{-0.19}$	$7.00 \to 8.09$
$\Delta m^2_{31}(\times 10^{-3}\mathrm{eV}^2)$[Normal]	$+2.473^{+0.070}_{-0.067}$	$+2.276 \to +2.695$
$\Delta m^2_{32}(\times 10^{-3}\mathrm{eV}^2)$[Inverted]	$-2.427^{+0.042}_{-0.065}$	$-2.649 \to -2.242$

sensitive to the mass hierarchy of the neutrino masses and the two different ranges are called *first quadrant* and *second quadrant* values. The data favor the first quadrant value over the second quadrant value in a normal hierarchy but there is no statistical preference between the two values in the case of inverted hierarchy [25].

2.5 Oscillations in presence of matter

Neutrino oscillations are affected by interactions in matter due to weak interactions, that we will discuss in Sec. 3.2, as discovered by Wolfenstein in 1978 [26]. Coherent forward-scattering mediated by a W boson contributes a term to the mixing matrix that is not present in vacuum and can be described as the potential [27]

$$\mathcal{V} = \sqrt{2} G_F n_e, \tag{2.5.1}$$

where G_F is the Fermi constant and n_e is the electron number density in the medium. This potential is actually the difference of the potentials for the neutrino flavors, that causes an aditional phase difference in the propagation. We can define the *refraction length* as

$$l_0 = \frac{\sqrt{2}\pi}{G_F n_e}, \tag{2.5.2}$$

which is similar to the oscillation length described before.

This potential modifies the evolution Hamiltonian as

$$H = H_0 + \mathcal{V}, \tag{2.5.3}$$

where H_0 is the Hamiltonian in vacuum. It also changes the eigenstates and eigenvalues so that in the two-flavor scenario Eq. (2.4.1) becomes

$$\begin{aligned} \nu_e &= \nu_{1m}\cos\theta_m + \nu_{2m}\sin\theta_m \\ \nu_\mu &= \nu_{2m}\cos\theta_m - \nu_{1m}\sin\theta_m, \end{aligned} \tag{2.5.4}$$

causing that also the mixing angle will depend on matter density and neutrino energy.

If we plot the dependance of the parameter $\sin^2 2\theta_m$ on the ratio of oscillation lenght over refraction lenght

$$x \equiv \frac{l_\nu}{l_0} = \frac{2EV}{\Delta m^2}, \tag{2.5.5}$$

we can see that it presents a *resonant* behaviour (Fig. 2.3). The mixing becomes maximal

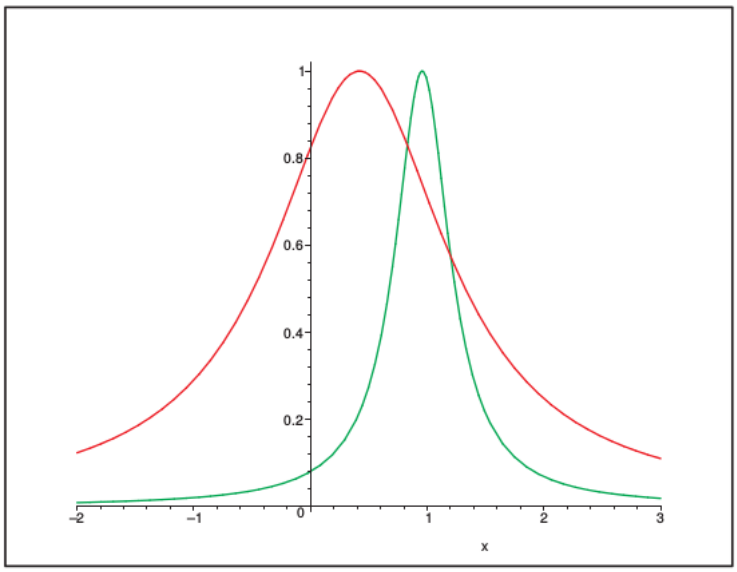

Figure 2.3: The dependence of the effective mixing parameter $\sin^2 2\theta_m$ on the ratio $x = l_\nu/l_0$ for two different values of the vacuum mixing: $\sin^2 2\theta = 0.825$ (red) which corresponds to the LMA solution and $\sin^2 2\theta = 0.08$ (green) which is at the upper bound on 1-3 mixing. The semi-plane $x < 0$ corresponds to the antineutrino channel. Credit: [27]

($\sin^2 2\theta_m = 1$) at the resonance condition $\theta_m = \pi/4$ so that:

$$l_\nu = l_0 \cos 2\theta. \tag{2.5.6}$$

For small vacuum mixing angles we see that the oscillation length becomes a good approximation of the refraction length. However, for large angles this does not hold and we find again a variation of the frequencies. Independently of the vacuum mixing, the resonance has physical meaning both for small and large mixing angles. The flavor mixing is maximal and the level splitting is minimal, so that in a *uniform* medium (constant mixing θ_m) the oscillation length is maximal. In this kind of medium, the flavors of the eigenstates do not change as well as the admixtures or mass proportions. This means

that ν_{1m} and ν_{2m} are the eigenstates of propagation and that $\nu_{1m} \leftrightarrow \nu_{2m}$ transitions do not occur. We can see this in Fig. 2.4 for the dependence of the eigenvalues H_{im} on the parameter x, or the level crossing scheme. Another remarkable characteristic is that the increase of the phase difference is monotonous.

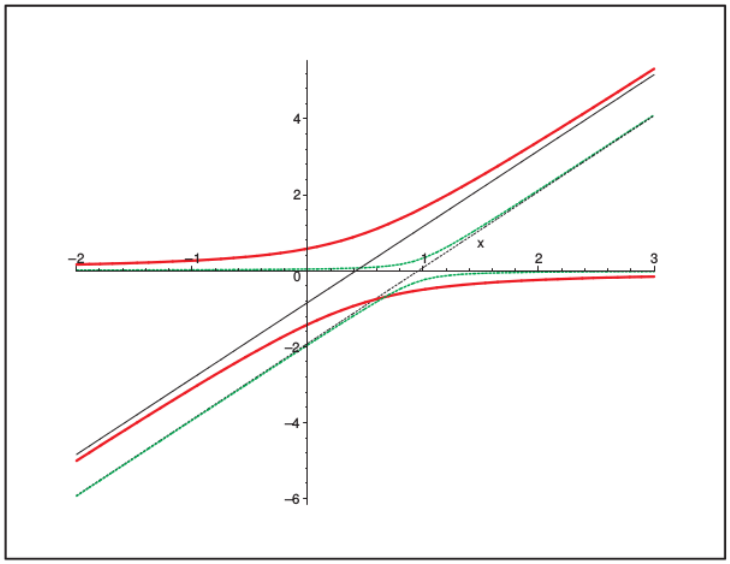

Figure 2.4: Level crossing scheme. Dependence of the eigenvalues of the Hamiltonian in matter, H_{1m} and H_{2m}, on the ratio $x = l_\nu/l_0$ for two different values of vacuum mixing $\sin^2 2\theta = 0.825$ (solid red) and $\sin^2 2\theta = 0.08$ (dashed green). Credit: [27]

Neutrinos crossing the Earth's mantle are a good example of oscillations in a medium with (nearly) constant density.

Oscillations in a medium with varying density are described by the **MSW effect** (Mikheyev-Smirnov-Wolfenstein) [26, 28]. Inside the Sun, for example, density varies following an exponential profile. The electron-neurinos interact with the electrons of the medium and forward scattering takes place. This process does not occur for muons or taus inside the Sun, so the hamiltonian interaction for electron-neutrinos is enhanced with respect to the other two flavors. The non-uniformity of the medium will make the Hamiltonian and the mixing angle dependant on time, so the (instantaneous) eigenstates are not the proper eigenstates of propagation aymore and the transitions $\nu_{1m} \leftrightarrow \nu_{2m}$ are allowed. However, if the density changes slowly enough, these transitions can be neglected. This is called *adiabaticity condition* and reads as

$$\gamma = \left| \frac{\theta'_m}{H_{2m} - H_{1m}} \right| \ll 1, \tag{2.5.7}$$

where $\theta'_m = \mathrm{d}\theta/\mathrm{d}r$ determines the energy of the transition and $|H_{2m} - H_{1m}|$ gives the energy gap between levels. The nonadiabatic evolution takes place in a localized region, with a center at the point of *maximal violation of adiabaticity* (PMVA). We will describe in more detail this process applied to the specific case of a Dark Matter profile in the Milky Way in Sec. 5.3.

Chapter 3

Neutrinos as spin 1/2 particles

After a descriptive picture of neutrinos, we will focus in this Chapter on their mathematical properties in the context of the Standard Model of particle physics (SM). We will discuss weak interactions, that are the responsible of the creation of neutrinos and antineutrinos. Then we will provide a detailed derivation of the electroweak unification in order to find a justification for the neutrino mass. We will finally explore different options beyond the SM that try to explain the hidden nature of neutrinos. Let us start with a formal representation of neutrinos as particles with half-integer spin, called *fermions*, and some of their properties. For a more detailed discussion and derivation we reccomend our main sources for this Chapter, [29, 30].

3.1 Spinors, helicity and chirality

We define *spinors* as the smallest non-trivial representation of the Lorentz group SO(3,1), with spin 1/2 and dimension two. Group theory is beyond the scope of this work, but we will include the *generators* of rotation ($\mathbf{J}$) and boost ($\mathbf{K}$) in the definitions of the two-component spinors

$$\phi_L : (1/2, 0), \quad \boldsymbol{J}^{(1/2)} = \boldsymbol{\sigma}/2, \quad \boldsymbol{K}^{(1/2)} = +i\boldsymbol{\sigma}, \tag{3.1.1}$$

$$\phi_R : (0, 1/2), \quad \boldsymbol{J}^{(1/2)} = \boldsymbol{\sigma}/2, \quad \boldsymbol{K}^{(1/2)} = -i\boldsymbol{\sigma}, \tag{3.1.2}$$

which we call *left-chiral* and *right-chiral* Weyl spinors. The components of $\boldsymbol{\sigma}$ are the Pauli matrices. These spinors transform by exponentiating the generators as $\exp(-i\boldsymbol{J}\boldsymbol{\alpha}+i\boldsymbol{K}\boldsymbol{\eta})$, where $\boldsymbol{\alpha}$ and $\boldsymbol{\eta}$ are the rotation angle and boost parameters, so that,

$$\phi_L \to \phi'_L = \exp\left[-\frac{i\boldsymbol{\sigma}\boldsymbol{\alpha}}{2} - \frac{\boldsymbol{\sigma}\boldsymbol{\eta}}{2}\right]\phi_L \equiv S_L\phi_L, \tag{3.1.3}$$

$$\phi_R \to \phi'_R = \exp\left[-\frac{i\boldsymbol{\sigma}\boldsymbol{\alpha}}{2} + \frac{\boldsymbol{\sigma}\boldsymbol{\eta}}{2}\right]\phi_R \equiv S_R\phi_R. \tag{3.1.4}$$

We can define *helicity* (h) as the phase $\mathrm{e}^{-ih\alpha}$ gained by a plane wave rotated an angle α around the propagation axis. Therefore, both spinors have helicity $h = 1/2$. They transform the same way under rotations but opposite under boosts.

We cannot transform a right-chiral spinor into a left-chiral one (or viceversa) because $\mathbf{K}$ transforms as a polar vector under parity change but $\mathbf{J}$ transforms as an axial vector.

This means that for $P\boldsymbol{x} = -\boldsymbol{x}$, the velocity changes sign $\boldsymbol{v} = -\boldsymbol{v}$ but the angular momentum remains invariant. Thus, (1/2,0) becomes (0,1/2) and so ϕ_L becomes ϕ_R (and viceversa). For this reason, we have to consider these spinors as components of a single object, called *four-spinor*, *Dirac spinor* or *bi-spinor*,

$$\psi = \begin{pmatrix} \phi_L \\ \phi_R \end{pmatrix}. \tag{3.1.5}$$

Dirac spinors satisfy the *Diract equation*,

$$(i\gamma^\mu \partial_\mu - m)\psi = 0, \tag{3.1.6}$$

where m is the mass of the particle and γ^μ are the 4×4 matrices,

$$\gamma^\mu = \begin{pmatrix} 0 & \sigma^\mu \\ \bar{\sigma}^\mu & 0 \end{pmatrix}, \tag{3.1.7}$$

satisfying

$$\begin{gathered} (\gamma^0)^2 = 1, \quad (\gamma^i)^2 = -1, \quad \gamma^\mu\gamma^\nu = -\gamma^\nu\gamma^\mu, \\ \gamma^0 = \gamma^{0\dagger} \qquad \text{and} \qquad \gamma^i = -\gamma^{i\dagger}, \end{gathered} \tag{3.1.8}$$

where $\mu \neq \nu$ and $i = 1, 2, 3$.

A specific combination of these matrices will be very relevant for our further analysis and therefore requires a special definition,

$$\gamma^5 \equiv \gamma_5 \equiv i\gamma^0\gamma^1\gamma^2\gamma^3. \tag{3.1.9}$$

Since the γ matrices and the Lorentz transformations are complex, the field ψ satisfying Eq. (3.1.6) is also complex and has four degrees of freedom. Dirac equation describes particles with spin 1/2, which carry 2 spin degrees of freedom ($2s$+1) for the particle and 2 more for the antiarticle. Thus, the number of components of ψ is the same as the number of physical states.

The Dirac equation becomes for plane waves with $m > 0$ and $E = p^0 = |\boldsymbol{p}| > 0$,

$$\begin{aligned} (\not{p} - m)u &= m(\gamma^0 - 1)u = 0, \\ (\not{p} + m)v &= m(\gamma^0 + 1)v = 0, \end{aligned} \tag{3.1.10}$$

where we introduce the Feynman slash ($\not{A} \equiv A_\mu\gamma^\mu$), so that $\not{p} = m\gamma^0$ in the rest frame, and the bi-spinor u for particles and v for antiparticles,

$$u(m,+) = \mathcal{N}\begin{pmatrix} 1 \\ 0 \\ 0 \\ 0 \end{pmatrix}, \quad u(m,-) = \mathcal{N}\begin{pmatrix} 0 \\ 1 \\ 0 \\ 0 \end{pmatrix}, \quad v(m,-) = \mathcal{N}\begin{pmatrix} 0 \\ 0 \\ 1 \\ 0 \end{pmatrix}, \quad v(m,+) = \mathcal{N}\begin{pmatrix} 0 \\ 0 \\ 0 \\ 1 \end{pmatrix}, \tag{3.1.11}$$

which are orthogonal,

$$\bar{u}(p,s)u(p,s') = \bar{v}(p,s)v(p,s') = \mathcal{N}^2\delta_{s,s'}. \tag{3.1.12}$$

We will normalise these spinors using the factor $\mathcal{N} = \sqrt{2m}$ that avoids singularities in the $m \to 0$ limit and makes the phase space volume identical to the one of bosons.

The Lagrangian density $\mathscr{L}$ can be expressed in terms of the Dirac field as

$$\mathscr{L} = \bar{\psi}(i\gamma^\mu \partial_\mu - m)\psi, \tag{3.1.13}$$

with ψ and $\bar{\psi}$ treated as independent fields. The Lagrane equation for $\bar{\psi}$ gives trivially the Dirac equation, while for ψ gives the adjoint. We can rearrange terms using the gamma matrices and the chiral representation to obtain the Dirac Lagrangian,

$$\mathscr{L} = i\phi_R^\dagger \sigma^\mu \partial_\mu \phi_R + i\phi_L^\dagger \bar{\sigma}^\mu \partial_\mu \phi_L - m(\phi_L^\dagger \phi_R + \phi_R^\dagger \phi_L). \tag{3.1.14}$$

All these terms are Lorentz invariant, so the Dirac equation is also Lorentz invariant. The mass terms are Lorentz scalars invariant under parity transformations, as well as the combinations of the kinetic energies of ϕ_L and ϕ_R.

We can also express the Dirac Lagrangian in the chiral representation by splitting any field ψ that is solution to the Dirac equation as

$$\psi_L = \tfrac{1}{2}(1 - \gamma^5)\psi \quad \text{and} \quad \psi_R = \tfrac{1}{2}(1 + \gamma^5)\psi, \tag{3.1.15}$$

to obtain

$$\mathscr{L} = i\bar{\psi}_L \partial\!\!\!/ \psi_L + i\bar{\psi}_R \partial\!\!\!/ \psi_R - m(\bar{\psi}_L \psi_R + \bar{\psi}_R \psi_L). \tag{3.1.16}$$

We can then identify the Dirac bi-spinors $\psi_{L/R}$ with the Weyl spinors $\phi_{R/L}$ at Eq. (3.1.14) as

$$\psi_L = \begin{pmatrix} \phi_L \\ 0 \end{pmatrix} \quad \text{and} \quad \psi_R = \begin{pmatrix} 0 \\ \phi_R \end{pmatrix}, \tag{3.1.17}$$

so we can define the left- and right-chiral components of any Dirac field in an arbitrary representation. The mass term that mixes lef- and right-chiral fields is called *Dirac mass* and is also invariant under chiral transformations. This term will be very relevant in our discussion about neutrino masses.

The helicity operator measures the projection of the spin of a particle on its momentum and commutes with the Dirac Hamiltonian because there is no orbital angular momentum in the direction of propagation. Particles with positive helicity are called *right-handed* and those with negative helicity are called *left-handed*. For massive particles, this quantity is frame-dependand because h changes sign if we choose a frame that moves in the direction of propagation of the particle but faster, so that the particle moves in the opposite direction. We cannot find such a frame for massless particles and thus helicity becomes a Lorentz invariant. This property is extremely relevant in our topic because neutrinos (as we know them up to now) are *only* left-handed, while antineutrinos are *only* right-handed. If the antagonic particles exist, they do not interact following the laws we know and the literature refers to them as *sterile neutrinos*. Helicity and chirality can then be understood as complementary. The first state is conserved and frame-dependent, while the second is frame-independent but not conserved.

3.2 Weak interactions

Neutrino emission is an exclusive characteristic of weak interactions, which are mediated by heavy *intermediate vector bosons*. Their measured masses are [31]

$$M_{W^\pm} = 80.385 \pm 0.015 \text{ GeV}, \qquad M_Z = 91.1876 \pm 0.0021 \text{ GeV}. \tag{3.2.1}$$

Since they have spin $s = 1$, they also have three polarization states $m_s = 1,\ 0,\ -1$, while massless particles as photons or gluons have two. Therefore we only impose the Lorentz condition to the polarization vector ϵ^μ

$$\epsilon^\mu p_\mu = 0 \tag{3.2.2}$$

to reduce the number of free parameters from 4 to 3. The resulting propagator is therefore

$$\frac{-i(g_{\mu\nu} - q_\mu q_\nu / M_V^2)}{q^2 - M_V^2} \tag{3.2.3}$$

The weak force is the only one of the four fundamental interactions that change flavor of particles and violate *charge-parity* symmetry. It affects all the fermions of the Standard Model as well as the Higgs boson.

We will discuss now the two different weak interactions based on their intermediate vector bosons: *charged current* (CC) and *neutral current* (NC) interactions.

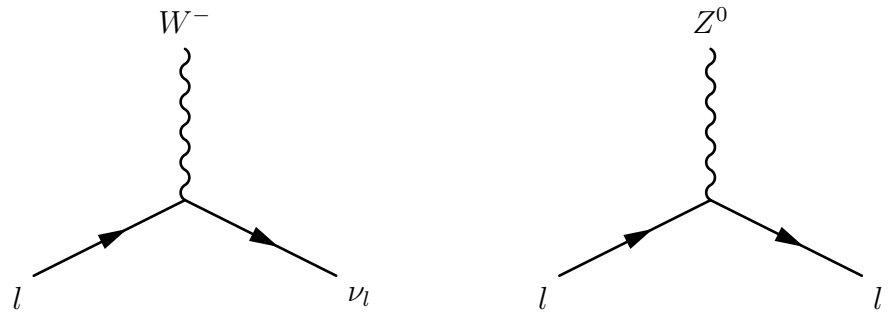

(a) (b)

Figure 3.1: Tree-level Feynman diagrams of the two fundamental weak interactions. Charged current CC (Fig.3.1a) and neutral current NC (Fig.3.1b).

3.2.1 Charged current interactions

The fundamental leptonic vertex of the charged weak interaction is shown in Fig.3.1a, where a charged lepton becomes its corresponding neutrino through the emission of a W^-. The reverse and crossed reactions are also allowed, exchanging particles for antiparticles where needed.

The vertex factor is always

$$\frac{-ig_w}{2\sqrt{2}}\gamma^\mu(1-\gamma^5), \tag{3.2.4}$$

where $g_w = \sqrt{4\pi\alpha_w}$ is the *weak coupling constant*. The term $(1-\gamma^5)$ repreents the *vector minus axial vector* $(V-A)$ nature of this interaction. Only γ^μ would be a *vector* coupling, while $\gamma^\mu\gamma^5$ would be an *axial vector* coupling. This term is resposible for the non conservation of parity, something characteristic of weak interactions.

As a relevant example of this interaction we will consider the inverse muon decay, as seen in Fig.(3.2), where a muon-neutrino interacts with an electron to produce a muon and an electron-neutrino. The momentum of the vector boson is $q = p_1 - p_3$ and we will

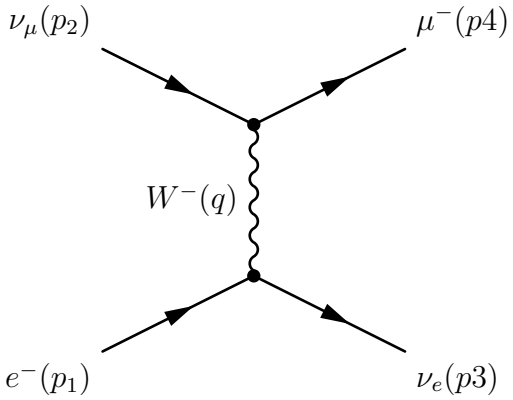

Figure 3.2: Inverse muon decay. A muon-neutrino interacts with an electron and produce a muon and an electron-neutrino through exchange of a W.

assumme that is much smaller than M_W^2 to simplify the propagator. Thus, the amplitude is,

$$\mathscr{M} = \frac{g_w^2}{8M_W^2}[\bar{u}(3)\gamma^\mu(1-\gamma^5)u(1)][\bar{u}(4)\gamma^\mu(1-\gamma^5)u(2)], \tag{3.2.5}$$

so that after applying Casimir's trick, evaluating the traces and neglecting neutrino masses we find,

$$\sum_{spins}|\mathscr{M}|^2 = 4\left(\frac{g_w}{M_W}\right)^4(p_1\cdot p_2)(p_3\cdot p_4). \tag{3.2.6}$$

To average over initial spins we need to consider that the electron has two spin states and neutrinos only have one. This gives us a factor 1/2. If we neglect the mass of the electron as well, we find in the CM frame

$$\left\langle|\mathscr{M}|^2\right\rangle = 8\left(\frac{g_w E}{M_W}\right)^4\left\{1-\left(\frac{m_\mu}{2E}\right)^2\right\}, \tag{3.2.7}$$

where E is the incident electron or neutrino energy. The differential cross section is isotropic and reads

$$\frac{d\sigma}{d\Omega} = \frac{1}{2}\left[\frac{g_w^2 E}{4\pi(M_W)^2}\right]^2\left\{1-\left(\frac{m_\mu}{2E}\right)^2\right\}, \tag{3.2.8}$$

and the total cross section is

$$\sigma = \frac{1}{8\pi}\left[\left(\frac{g_w}{M_W}\right)^2 E\right]^2 \left\{1 - \left(\frac{m_\mu}{2E}\right)^2\right\}. \tag{3.2.9}$$

Now we will focus our attention in some mechanisms that produce neutrinos as outgoing particles

Muon decay The reaction shown in fig. 3.3 is theoretically and experimentally the simplest of all weak processes. The amplitude associated is

$$\mathscr{M} = \frac{g_w^2}{8M_W^2}\left[\bar{u}(3)\gamma^\mu(1-\gamma^5)u(1)\right]\left[\bar{u}(4)\gamma^\mu(1-\gamma^5)v(2)\right] \tag{3.2.10}$$

from which we obtain

$$\langle|\mathscr{M}|^2\rangle = 2\left(\frac{g_w}{M_W}\right)^4 (p_1\cdot p_2)(p_3\cdot p_4). \tag{3.2.11}$$

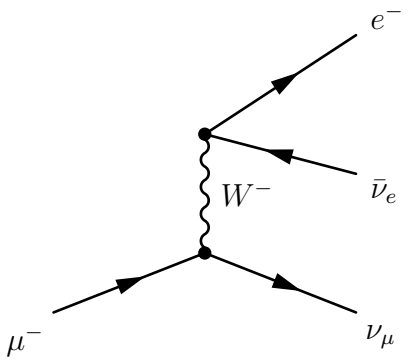

Figure 3.3: Decay of the muon into an electron, one neutrino and one antineutrino.

Pion decay This reaction may be studied as the scattering process of two quarks that are bound together, as seen in Fig. 3.4. The amplitude for any lepton family l has the form

$$\mathscr{M} = \frac{g_w^2}{8M_W^2}[\bar{u}(l)\gamma_\mu(1-\gamma^5)v(\nu)]F^\mu, \tag{3.2.12}$$

where F^μ is a form factor describing the interaction between the pion and the W. It has to be a four-vector to contract with the gamma matrix and can only be the momentum since the pion has spin zero. Therefore it must be a scalar times the momentum vector $F^\mu = f_\pi p^\mu$. Therefore we find

$$\left\langle|\mathscr{M}|^2\right\rangle = \left(\frac{g_w}{2M_W}\right)^4 f_\pi^2 m_l^2(m_\pi^2 - m_l^2). \tag{3.2.13}$$

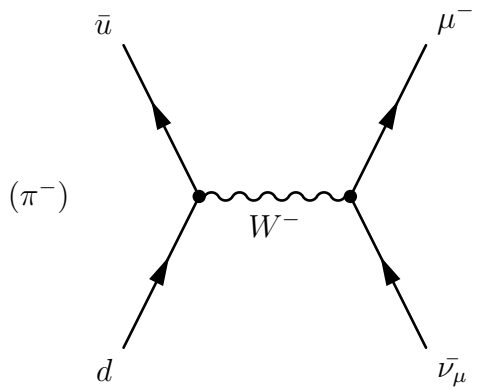

Figure 3.4: Pion decay.

The decay ratio is then described by the formula

$$\Gamma = \frac{S|\mathbf{p}|}{8\pi m_1} \left\langle |\mathcal{M}|^2 \right\rangle , \tag{3.2.14}$$

where $|\mathbf{p}|$ is the outgoing momentum expressed as

$$|\mathbf{p}| = \frac{1}{2m_\pi}(m_\pi^2 - m_l^2). \tag{3.2.15}$$

We find

$$\Gamma = \frac{f_\pi^2}{\pi m_\pi^3} \left(\frac{g_w}{4M_W} \right)^4 m_l^2 (m_\pi^2 - m_l^2)^2. \tag{3.2.16}$$

Since we ignore the value of the constant f_π we cannot calculate the lifetime of the pion. However, we can calculate an estimate for the ratio of the decay rate of the electron and muon channels as

$$\frac{\Gamma(\pi^- \to e^- + \bar{\nu}_e)}{\Gamma(\pi^- \to \mu^- + \bar{\nu}_\mu)} = \frac{m_e^2(m_\pi^2 - m_e^2)^2}{m_\mu^2(m_\pi^2 - m_\mu^2)^2} = 1.283 \times 10^{-4}. \tag{3.2.17}$$

It looks surprising that the electron channel is strongly suppressed in favour of the muon channel even though the mass difference is larger. However, we see in Eq. (3.2.16) that if the electron was indeed massless, the channel would be forbidden. This can also be expained through spin and helicity. The pion has spin 0 and therefore the antineutrino and the electron emerge with opposite spins and equal helicity. Antineutrinos are always right-handed, so the electron must also be right-handed. On the other hand, if the electron was trully massless, then the $1 - \gamma^5$ term in the weak vertex would only couple to left-handed electrons, in the same way as it only couples to left-handed, neutrinos therefore suppressing this pion decay channel. Experimental measurements of the helicity of the muons determined that they are always right-handed in this process, which confirms that antineutrinos are right-handed. The process for π^+ gave the opposite results, confirming that neutrinos are always left-handed.

Kaon decay The decay of this meson can serve as example of how heavier particles can decay through different mechanisms and produce neutrinos. The pure *leptonic decay* is a similar process as the pion decay shown in Fig. 3.4 where the difference is a *strange* quark

plus an *anti-up* quark instead of a *down* quark plus an *anti-up* to produce the W^-. The decay rate would then be the analog of Eq. (3.2.16) with the mass and the form factor of the kaon instead of the pion. Another source of neutrinos from the kaon would then be the *semi-leptonic* decay, where the $\bar{K}^0$ decays into a pion, a lepton and the corresponding antineutrino. The muon channel is shown in Fig. 3.5. The decay $\pi^- \to \pi^0 + e^- + \bar{\nu}_e$ would be another example of the same process.

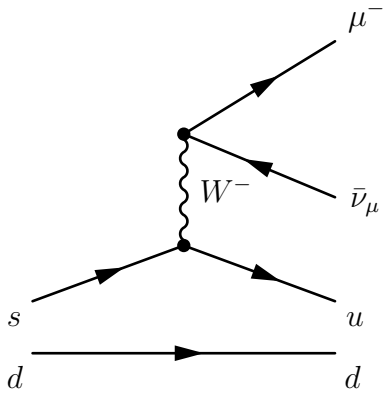

Figure 3.5: Decay of the $\bar{K}^0$ into a π^+, a muon and one antineutrino.

Neutron decay The neutron is a composite particle consisting of three quarks and its decay is really the decay of a d quark into a u quark so that the neutron becomes a proton, as shown in Fig. 3.6. Following the same procedure as before we would find that

$$\left\langle |\mathscr{M}|^2 \right\rangle = m_n \left(\frac{g_w}{M_W} \right)^4 |\mathbf{p}_2| \left(m_n^2 - m_p^2 - m_e^2 - 2m_n |\mathbf{p}_2| \right), \tag{3.2.18}$$

so that the differential decay rate as a function of the outgoing eletron energy is

$$\frac{d\Gamma}{dE} = \frac{1}{\pi^3} \left(\frac{g_w}{2M_W} \right)^4 E\sqrt{E^2 - m_e^2}[(m_n - m_p) - E]^2. \tag{3.2.19}$$

Integrating over the electron energies we find the total decay rate

$$\Gamma = \frac{1}{4\pi^3} \left(\frac{g_w}{2M_W} \right)^4 m_e^5 \left[\frac{1}{15}(2a^4 - 9a^2 - 8)\sqrt{a^2 - 1} + a \ \ln(a + \sqrt{a^2 - 1}) \right], \tag{3.2.20}$$

where we used

$$a \equiv \frac{m_n - m_p}{m_e}. \tag{3.2.21}$$

Inserting the physical values we find the neutron lifetime

$$\tau = \frac{1}{\Gamma} = 1318 \text{ s}, \tag{3.2.22}$$

which does not really agree with the experimental data $\tau = 880.3 \pm 1.1$ seconds (*Particle Physics Booklet* 2014 [31]). This is due to the inner structure of the neutron, that does

not allow us to treat this decay as simple as we did. We must take into consideration some corrections to the weak vertex caused by the strong interactions between the quarks, such as

$$(1 - \gamma^5) \to (c_V - c_A\gamma^5), \tag{3.2.23}$$

where c_V is the correction to the vector 'weak charge' and c_A is the correction to the axial vector part. Experimental results show that,

$$c_V = 1.000, \qquad c_A = 1.270 \pm 0.003. \tag{3.2.24}$$

This means that the *vector* weak charge is not modified by the strong interactions inside the neutron, while the *axial vector* part is slightly altered. These are called 'Conserved Vector Current' (CVC) and 'Partially Conserved Axial Current' (PCAC) hypotheses. CVC was included in the Standard Model and the value of c_V accepted as 1 exactly.

Inserting these values in the previous equations we find that the decay rate changes by a factor of 1.46 so that the lifetime is,

$$\tau = \frac{1316 \text{ s}}{1.46} = 901 \text{ s}. \tag{3.2.25}$$

This is a better approximation but not an improvement, since there are other corrections to be taken into consideration such as the $d \to u + W$ quark vertex, that carries a factor involving the mixing angles of the quarks, or a small Coulomb correction due to the attraction of the proton and the electron in the final state, but we will not go into further detail.

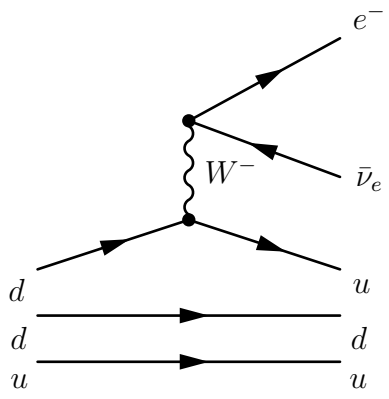

Figure 3.6: Decay of the neutron into a proton, an electron and one antineutrino.

Other sources of neutrinos are for example nuclear fusion reactions in the Sun and other stars, such as the first stage of proton-proton fusion

$$p^+ + p^+ \to {}^2_1\text{H} + e^+ + \nu_e, \tag{3.2.26}$$

and the carbon cycle

$${}^{13}_{7}\text{N} \to {}^{13}_{6}\text{C} + e^+ + \nu_e, \tag{3.2.27}$$

as well as much more energetic processes like Supernova explosions of very massive stars that collapse under their own gravity. During this process, the electrons of the star core are forced into the nucleus via inverse β-decay and electron-neutrinos are released.

3.2.2 Neutral current interactions

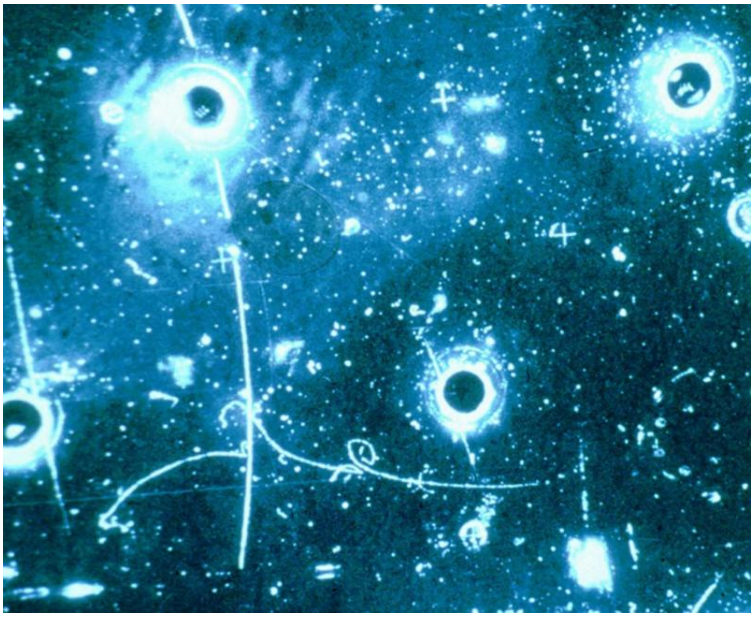

Figure 3.7: The first example of a single-electron neutral current. An incoming antineutrino knocks an electron towards the left, creating a characteristic electronic shower with electron-positron pairs. Credit: Gargamelle/CERN.

Most neutral weak processes are hidden by the equivalent electromagnetic one since the photon can couple to everything the Z^0 does and at low energies the photon mechanism clearly dominates. Therefore, neutrino scattering was used to confirm the existence of a neutral weak current, since neutrinos do not couple to the photon. In 1973, the GARGAMELLE experiment at CERN [32] was able to produce the first image of a neutral current interaction between a muon-antineutrino and an electron (Fig.3.7),

$$\bar{\nu}_\mu + e^- \rightarrow \bar{\nu}_\mu + e^-, \tag{3.2.28}$$

that suggested a neutral mediator as the theoretically predicted Z^0 (Fig.3.8).

There were also observed some neutrino-nucleon scattering events that revealed the neutral neutrino-quark interaction. The cross sections were much smaller than the corresponding charged current events, so that it needed to be a new interaction and not higher-order processes.

The fundamental vertex of a neutral current interaction is shown in fig.3.1b, where the same lepton enters and exits the reaction.

The vertex factor is in this case

$$\frac{-ig_z}{2}\gamma^\mu(c_V^f - c_A^f\gamma^5), \tag{3.2.29}$$

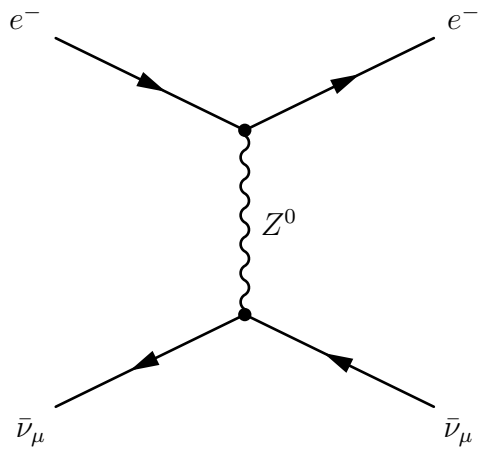

Figure 3.8: Neutral current interaction between an incoming muon-antineutrino and an electron.

where g_z is the neutral coupling constant and the vector and axial vector corrections c_V^f and c_A^f depend on the fermion involved in the reaction. In the unified electroweak theory (that we will discuss in section 3.3) all these parameters are determined by the weak mixing angle or Weinberg angle θ_w, which also relates the electromagnetic and weak coupling constants,

$$g_w = \frac{g_e}{\sin\theta_w}, \qquad g_z = \frac{g_e}{\sin\theta_w \cos\theta_w}, \tag{3.2.30}$$

where g_e is determined by the charge of the electron ($g_e = e\sqrt{4\pi}$). The vector boson masses are also related by this angle as,

$$M_W = M_Z \cos\theta_w. \tag{3.2.31}$$

As an example of this kind of interactions, we will look at the elastic neutrino-electron scattering process. We can use the Feynman diagram shown in Fig. 3.8 bearing in mind that the incoming particle is a neutrino instead of an antineutrino. This will also serve as a comparison with the charged current interaction shown in Fig. 3.2.

The amplitude of this process is

$$\mathscr{M} = \frac{g_z^2}{8M_Z^2}[\bar{u}(p_3)\gamma^\mu(1-\gamma^5)u(p_1)][\bar{u}(p_4)\gamma_\mu(c_V - c_A\gamma^5)u(p_2)], \tag{3.2.32}$$

so that

$$\left\langle|\mathscr{M}|^2\right\rangle = 2\left(\frac{g_z E}{4M_Z}\right)^4 \left[(c_V + c_A)^2 + (c_V - c_A)^2\cos^4\frac{\theta}{2}\right], \tag{3.2.33}$$

where E is the incoming neutrino or electron energy, θ is the scattering angle between incoming and outgoing directions in the CM frame and we have used that c_V and c_A for the neutrino are 1/2 [2]. The cross section then reads

$$\sigma = \frac{2}{3\pi}\left(\frac{g_z}{2M_Z}\right)^4 E^2(c_V^2 + c_A^2 + c_V c_A). \tag{3.2.34}$$

The theoretically predicted value was $\sigma \sim 10^{-41}$ cm^2/electron at 1 GeV[32]. Inserting the values from Table 9.1 in [2] we find a ratio of

$$\frac{\sigma(\nu_\mu + e^- \to \nu_\mu + e^-)}{\sigma(\nu_\mu + e^- \to \nu_e + \mu^-)} = \frac{1}{4} - \sin^2\theta_w + \frac{4}{3}\sin^4\theta_w = 0.0900. \tag{3.2.35}$$

This result show how unlikely these processes are to happen and justify the low number of neutrino scattering events inside detectors and the time invested in collecting useful data.

3.3 Electroweak theory

Fermi tried to explain the nuclear β-decay through a current-current interaction between two fermions,

$$\mathscr{L}_{Fermi} = \frac{G_F}{\sqrt{2}} J^\mu(x) J_\mu(x). \tag{3.3.1}$$

When parity violation was found in weak interactions, the leptonic current was then described as a $V - A$ interaction,

$$J_\mu(x) = \bar{\psi}_e \gamma_\mu (1 - \gamma^5)\psi_\nu + h.c. \tag{3.3.2}$$

However, this theory is included in the class of non-renormalisable theories and further efforts were demanded. The first attempt to construct a renormalisable gauge theory was the introduction of intermediate vector bosons $W^\pm$ with mass m_W. The charged current interaction can then be written using doublets of left-handed fermions,

$$\begin{pmatrix} \nu_e \\ e \end{pmatrix}_L \quad \text{and} \quad \begin{pmatrix} u \\ d \end{pmatrix}_L. \tag{3.3.3}$$

This doublet structure suggests the gauge group SU(2) for weak interactions, which is often called *weak isospin*. Only left-handed fermions interact this way and therefore the goup is usually denoted $SU(2)_L$, while right-handed fermions transform as singlets. We can now associate the vector bosons $W^\mp$ with the ladder operators $\tau_\mp = (\tau_1 \pm i\tau_2)/\sqrt{2}$ so the interaction becomes

$$\mathscr{L}_{Fermi} = \frac{G_F}{2\sqrt{2}} \begin{pmatrix} \bar{\nu}_e & \bar{e} \end{pmatrix}_L \left(\tau^+ W_\mu^- + \tau^- W_\mu^+\right) \gamma^\mu \begin{pmatrix} \nu_e \\ e \end{pmatrix}_L. \tag{3.3.4}$$

For an electroweak unification, we need to identify the τ_3 with the photon, but there are three inconvenients:

- The fermion mass term $m(\bar{\psi}_R\psi_L + \bar{\psi}_L\psi_R)$ is not gauge invariant.
- The generators of SU(2) are traceless; multiplets must have zero net charge.
- The currents generated by $\tau_\pm$ should have $V - A$ structure but the electromagnetic current has to be a pure vector current.

Glashow suggested that the gauge group of weak and electromagnetic interactions is the product of two groups [33], while Weinberg and Salam included the idea of *spontaneous symmetry breaking* using the Higgs mechanism [34, 35] so that

$$SU(2)_L \otimes U(1)_Y \to U(1)_{EM}, \tag{3.3.5}$$

where Y stands for hypercharge. Let us now go into some more detail about this mechanism.

A $SU(2) \otimes U(1)$ gauge theory contains four gauge bosons but only one should remain massless. Using a complex SU(2) doublet to break the gauge symmetry would add four real degrees of freedom, of which three will become longitudinal degrees of freedom for the three massive gauge bosons and one physical Higgs field remains. This complex scalar SU(2) doublet is

$$\mathbf{\Phi} = \begin{pmatrix} \phi^+ \\ \phi^0 \end{pmatrix} = \frac{1}{\sqrt{2}} \begin{pmatrix} \phi_1 + i\phi_2 \\ \phi_3 + i\phi_4 \end{pmatrix}. \tag{3.3.6}$$

The Lagrangian

$$\mathscr{L} = (\partial_\mu \mathbf{\Phi})^\dagger (\partial^\mu \mathbf{\Phi}) + \mu^2 \mathbf{\Phi}^\dagger \mathbf{\Phi} - \lambda \left(\mathbf{\Phi}^\dagger \mathbf{\Phi}\right)^2 \tag{3.3.7}$$

is invariant under global SU(2) and U(1) transformations of $\mathbf{\Phi}$,

$$\mathbf{\Phi} \to \exp\left\{\tfrac{i\boldsymbol{\alpha}\cdot\boldsymbol{\tau}}{2}\right\} \mathbf{\Phi} \quad \text{and} \quad \mathbf{\Phi} \to \exp\left\{\tfrac{i\theta Y}{2}\right\} \mathbf{\Phi}, \tag{3.3.8}$$

where we have chosen the Pauli matrices $\boldsymbol{\tau}$ as generators for the weak isospin transformations. The U(1) charge Y can take any value, so we choose $Y(\mathbf{\Phi}) = 1$ with a factor $1/2$ added by convention.
We choose the vacuum expectation value in the ϕ^0 direction to avoid an electrically charged vacuum,

$$\langle 0|\mathbf{\Phi}|0\rangle = \begin{pmatrix} 0 \\ \frac{v}{\sqrt{2}} \end{pmatrix}. \tag{3.3.9}$$

Electroweak symmetry breaking should leave $U_{em}(1)$ invariant and this is achieved using the combination $\mathbf{1} + \tau_3$,

$$\delta\mathbf{\Phi} = i\epsilon(\mathbf{1} + \tau_3)\mathbf{\Phi} = i\epsilon \begin{pmatrix} 2 & 0 \\ 0 & 0 \end{pmatrix} \begin{pmatrix} 0 \\ \frac{v}{\sqrt{2}} \end{pmatrix} = 0. \tag{3.3.10}$$

In the weak isospin space, the hypercharge generator is the identity matrix, so we should associate the electric charge Q to the combination $Y + \tau_3$. In this fashion we expect the photon as a superposition of the $U(1)_Y$ abelian gauge boson and the third component of the $SU(2)_L$ non-abelian gauge boson. Applying $Q \propto Y + \tau_3$ to the upper component ϕ^+ of the Higgs doublet we find the Gell-Mann−Nishijima relation $2Q = Y + \tau_3$.

Now we gauge the model via covariant derivatives,

$$\partial^\mu \mathbf{\Phi} \to D^\mu \mathbf{\Phi} = \left(\partial^\mu + \frac{ig}{2}\, \boldsymbol{\tau}\cdot \boldsymbol{W}^\mu + \frac{ig'}{2} B^\mu\right) \mathbf{\Phi}, \tag{3.3.11}$$

suppressing a unit matrix in isospin space in from of ∂^μ and B^μ and introducing the couplings g and g' for the two groups. We obtain the field-strengths for the three $SU(2)_L$ gauge fields $\boldsymbol{W}^\mu$ and the $U(1)_Y$ field B^μ as

$$F_a^{\mu\nu} = \partial^\mu W_a^\nu - \partial^\mu W_a^\mu - g\epsilon_{abc} W_b^\mu W_c^\nu \tag{3.3.12}$$

$$G^{\mu\nu} = \partial^\mu B^\nu - \partial^\nu B^\mu, \tag{3.3.13}$$

where ϵ_{abc} is a completely antisymmetric tensor that corresponds to the structure constants of SU(2). In this way, we find the Lagrangian describing the Higgs gauge sector as

$$\mathscr{L} = -\frac{1}{4}F^2 - \frac{1}{4}G^2 + (D_\mu \mathbf{\Phi})^\dagger (D^\mu \mathbf{\Phi}) - V(\mathbf{\Phi}). \tag{3.3.14}$$

We are interested in the mass spectrum of physical particles and therefore we spontaneously break this theory using unitary gauge. We can achieve only one physical scalar field if we use polar coordinates for the lower component, $\phi^0 = \rho e^{i\theta}$ and setting $\phi^+ = \theta = 0$ by a SU(2) unitary transformation, which only changes the longitudinal components of the SU(2) gauge bosons. We separate ρ into the vev $v = \sqrt{\mu^2/\lambda}$ and fluctuations $h(x)$,

$$\mathbf{\Phi} = \begin{pmatrix} 0 \\ \frac{1}{\sqrt{2}}(v + h(x)) \end{pmatrix} = \frac{v+h}{\sqrt{2}} \begin{pmatrix} 0 \\ 1 \end{pmatrix} \equiv \frac{v+h}{2}\chi. \tag{3.3.15}$$

Inserting the part containing v into Eq. (3.3.14) we find the mass terms

$$\mathscr{L}_m = \frac{v^2}{2}\chi^\dagger \left(\frac{g}{2}\boldsymbol{\tau}\cdot\boldsymbol{W}^\mu + \frac{g'}{2}B^\mu\right)\left(\frac{g}{2}\boldsymbol{\tau}\cdot\boldsymbol{W}_\mu + \frac{g'}{2}B_\mu\right)\chi. \tag{3.3.16}$$

Using $(\boldsymbol{\tau}\cdot\boldsymbol{W})^2 = \boldsymbol{W}^2$ and $\chi^\dagger\boldsymbol{\tau}\cdot\boldsymbol{W}^\mu\chi = -W_3^\mu$ after multiplying out the brackets, we find

$$\mathscr{L}_m = \frac{v^2}{2}\left[\frac{g^2}{4}(W_1^2 + W_2^2 + W_3^2) + \frac{g'^2}{4}B^2 - \frac{gg'}{2}W_3^\mu B_\mu\right]. \tag{3.3.17}$$

We see that the neutral fields W_3^μ and B^μ are connected so we rewrite the mass term as

$$\mathscr{L}_m = \frac{g^2v^2}{8}(W_1^2 + W_2^2) + \frac{v^2}{8}(gW_3^\mu - g'B^\mu)^2. \tag{3.3.18}$$

We can identify the two fields in the first bracket with the gauge bosons from the charged current interaction in the Fermi theory,

$$W^\pm = \frac{1}{\sqrt{2}}(W_1 \mp iW_2)^2. \tag{3.3.19}$$

In the same way, we will identify the second bracket with a new neutral massive gauge boson called Z that is a mixture of the W_3 and B fields,

$$Z^\mu = \frac{1}{\sqrt{g^2+g'^2}}(gW_3^\mu - g'B^\mu) = \cos\theta_W W_3^\mu - \sin\theta_W B^\mu, \tag{3.3.20}$$

where θ_W is the Weinberg angle, which parametrises the mixing of B and W_3. The mixing disappears for $\theta_W = 0$ and the hypercharge equals the electric charge.

We can also identify the massless photon with the combination of W_3 and B orthogonal to Z since it does not appear in the mass Lagrangian,

$$A^\mu = \frac{1}{\sqrt{g^2+g'^2}}(g'W_3^\mu + gB^\mu) = \sin\theta_W W_3^\mu + \cos\theta_W B^\mu. \tag{3.3.21}$$

The mass Lagrangian in terms of physical fields then becomes

$$\mathscr{L}_m = \frac{1}{2}m_W^2 + W_\mu^+ W^{-\mu} + \frac{1}{2}m_Z^2 Z_\mu Z^\mu, \tag{3.3.22}$$

where the boson masses are

$$m_W = \tfrac{gv}{2}, \quad m_Z = \tfrac{\sqrt{(g^2+g'^2)}v}{2} = \tfrac{m_w}{\cos\theta_W} \quad \text{and} \quad m_A = 0, \tag{3.3.23}$$

as function of the unknown values of the coupling constants g and g' and the vev v. We see that the mass ratio of the gauge bosons is fixed at tree level by the Weinberg angle

$$\frac{m_W}{m_Z} = \cos\theta_W. \tag{3.3.24}$$

As mentioned in Section 3.2.2, g and g' should be related to the electromagnetic coupling e and the Weinberg angle θ_W. To find that, we will insert the physical fields Z^μ and A^μ in the covariant derivative (Eq. (3.3.11)) by inverting Eqs. (3.3.20) and (3.3.21)

$$\begin{aligned} gW_3^\mu\tau_3 + g'B^\mu\mathbf{1} &= g(\cos\theta_W Z^\mu + \sin\theta_W A^\mu)\mathbf{1} + g'(-\sin\theta_W Z^\mu + \cos\theta_W A^\mu)\tau_3 \\ &= (g\sin\theta_W\tau_3 + g'\cos\theta_W\mathbf{1})A^\mu + (g\cos\theta_W\tau_3 - g'\sin\theta_W\mathbf{1})Z^\mu. \end{aligned} \tag{3.3.25}$$

Using $\tan\theta_W = g'/g$ we find

$$g\frac{W_3^\mu\tau_3}{2} + g'\frac{B^\mu\mathbf{1}}{2} = \frac{1}{2}g\sin\theta_W(\tau_3+\mathbf{1})A^\mu + \frac{g}{2\cos\theta_W}\left(\tau_3 - \sin^2\theta_W(\tau_3+\mathbf{1})\right)Z^\mu. \tag{3.3.26}$$

We assigned the electric charge to the upper component ϕ^+ so that $\mathcal{D}_\mu\mathbf{\Phi}$ implies

$$e = g\sin\theta_W = g'\cos\theta_W, \tag{3.3.27}$$

while the lower component ϕ^0 stays neutral.

3.4 Fermion mass and flavor mixing

In this section we will describe the mechanism that provides mass to fermions. The term in the Lagrangian associated to fermion mass

$$m(\bar\psi_R\psi_L + \bar\psi_L\psi_R) \tag{3.4.1}$$

needs to be gauge invariant. Therefore we need the parameter m to become a SU(2) doublet. If we introduce a Yukawa coupling $y_f = m/v$ between the lepton doublet L, the scalar doublet Φ and the lepton singlet e_R,

$$\mathscr{L}_Y = -y_f\left(\bar L\Phi e_R + \bar e_R\Phi^\dagger L\right), \tag{3.4.2}$$

we obtain a SU(2) invariant term. Knowing that $Y(\Phi) = 1$ and $Y(L) = -1$, we can also obtain a $\mathrm{U}_Y(1)$ invariant mass term if the lepton singlet has hypercharge $Y(e_R) = -2$. This satisfies the Gell-Mann-Nishijima relation $2Q = Y + 2T_3$. This coupling generates masses and Yukawa interactions between the fermions and the Higgs. After inserting the vacuum expectation of the Higgs, we find a Dirac mass term in the form

$$\begin{aligned} \mathscr{L}_m &= -\frac{y_f v}{\sqrt{2}}\left[\begin{pmatrix}\bar\nu_e & \bar e\end{pmatrix}_L\begin{pmatrix}0\\1\end{pmatrix}e_R + \bar e_R\begin{pmatrix}0 & 1\end{pmatrix}_L\begin{pmatrix}\nu_e\\ e\end{pmatrix}_L\right] \\ &= -m_f\left(\bar e_L e_R + \bar e_R e_L\right) = -m_f\bar e e, \end{aligned} \tag{3.4.3}$$

and we generate the masses for the down-like fermions with $\tau_3 = -1/2$ like the electron. For the up-like fermions we need the charge conjugated Higgs doublet $i\tau_2\Phi^*$. In order to

justify this, we show how quarks and anti-quarks transform under $\mathrm{SU}(2)_L$. The quarks transform as

$$q \to q' = Uq = \exp\left\{-\frac{i\boldsymbol{\alpha}\cdot\boldsymbol{\tau}}{2}\right\} q, \tag{3.4.4}$$

with

$$q = \begin{pmatrix} u \\ d \end{pmatrix}, \tag{3.4.5}$$

while the charged conjugated reads

$$q^{*'} = U^* q^* = \exp\left\{-\frac{i\boldsymbol{\alpha}\cdot\boldsymbol{\tau}^*}{2}\right\} \begin{pmatrix} \bar{u} \\ \bar{d} \end{pmatrix}. \tag{3.4.6}$$

The bar denotes antiparticles and the conjugated Pauli matrices are

$$\tau_1^* = \tau_1, \qquad \tau_2^* = -\tau_2, \qquad \tau_3^* = \tau_3. \tag{3.4.7}$$

The set $\left\{\frac{\tau_1}{2}, -\frac{\tau_2}{2}, \frac{\tau_3}{2}\right\}$ satisfies the same Lie algebra as the original set and is an appropriate basis for the antiquarks. This 2* representation and the original 2 representation must be unitary equivalent . For any unitary matrix V,

$$V \ \exp\left\{-\frac{i\boldsymbol{\alpha}\cdot\boldsymbol{\tau}}{2}\right\} \ V^{-1} = \exp\left\{\frac{i\boldsymbol{\alpha}\cdot\boldsymbol{\tau}}{2}\right\}. \tag{3.4.8}$$

This expression simplifies to

$$V\,(-\boldsymbol{\tau}^*)\,V^{-1} = \boldsymbol{\tau} \tag{3.4.9}$$

for infinitesimal $|\boldsymbol{\alpha}|$, so that $V = i\tau_2$. Therefore we obtain

$$V \begin{pmatrix} \bar{u} \\ \bar{d} \end{pmatrix} = \begin{pmatrix} \bar{d} \\ -\bar{u} \end{pmatrix}. \tag{3.4.10}$$

This doublet transforms in the same way as the 2 representation, so we can use $\mathrm{i}\tau_2\phi^*$ to generate Dirac masses for neutrinos and up-like quarks.

The coupling y_f and therefore the mass m_f for the three generations of lepton and quarks are 3x3 arbitrary matrices in flavor space, $\boldsymbol{y}$ and $\boldsymbol{m}$. There is no particular reason for $\mathbf{y}$ to be diagonal or hermitian so it can be diagonalized by a biunitary transformation such as

$$\boldsymbol{S^\dagger m T} = \boldsymbol{m_D}, \tag{3.4.11}$$

where $\boldsymbol{S}$ and $\boldsymbol{T}$ are unitary matrices and $\boldsymbol{m_D}$ is diagonal and positive. Following this, the weak eigenstates $\boldsymbol{\psi} = \{\psi_e, \psi_\mu, \psi_\tau\}$ transform into mass eigenstates $\boldsymbol{\psi'} = \{\psi_1, \psi_2, \psi_3\}$ as

$$\bar{\boldsymbol{\psi}}_{\boldsymbol{L}} \boldsymbol{m} \boldsymbol{\psi}_{\boldsymbol{R}} = \bar{\boldsymbol{\psi}}_{\boldsymbol{L}} \boldsymbol{S} \boldsymbol{S^\dagger} \boldsymbol{m} \boldsymbol{T} \boldsymbol{T^\dagger} \boldsymbol{\psi}_{\boldsymbol{R}} = \bar{\boldsymbol{\psi}'}_{\boldsymbol{L}} \boldsymbol{m_D} \boldsymbol{\psi'_R}. \tag{3.4.12}$$

The problem we encounter now is that these new eigenstates are not diagonal in the interaction basis and this will produce *flavor mixing*. Evaluating the charged weak current J^μ with the mass eigenstates,

$$J^\mu = \bar{\boldsymbol{\nu}}_{\boldsymbol{L}} \gamma^\mu \boldsymbol{e_L} = \bar{\boldsymbol{\nu}}'_{\boldsymbol{L}} \gamma^\mu \boldsymbol{S}^\dagger_{\boldsymbol{\nu}} \boldsymbol{S}_{\boldsymbol{e}} \boldsymbol{e}'_{\boldsymbol{L}}, \tag{3.4.13}$$

we find that there will be only one observable, $\boldsymbol{U} \equiv \boldsymbol{S}^\dagger_{\boldsymbol{\nu}} \boldsymbol{S}_{\boldsymbol{e}}$. This gives us some freedom to choose mixing only for neutrinos and down-like quarks, meaning $\boldsymbol{S_e} = \mathbf{1}$ and $\boldsymbol{U} = \boldsymbol{S_\nu}$. The

$\boldsymbol{U}$ matrices for neutrinos and quarks are called respectively MNS-matrix (Eq. (2.4.12)) and CKM-matrix.

If we choose the neutrino masses to be zero following the SM, then $\boldsymbol{S_\nu}$ is abritrary and we can set it equal to $\boldsymbol{S_e}$, so that $\boldsymbol{U} = 1$ and no mixing occurs. This would lead to the conservation of lepton number of each generation, which in turn guarantees that perturbation loop theory does not generate neutrino masses. However, the observed non-zero masses of the neutrinos confirm that leptons mix via the MNS-matrix and thus only the total lepton number is a conserved quantity in the SM.

3.5 Dirac vs. Majorana Neutrinos

Dirac fermions are massive particles that carry a conserved U(1) charge, which allows us to distinguish between particles and anti-particles. Neutrinos are the only particles of the SM that do not carry electric charge and traditionally they were considered massless. Let us describe now both cases independently.

First we will consider charged massless particles, called **Weyl fermions**. In the chiral representation, the Dirac equation

$$\begin{pmatrix} -m & i(\partial_0 + \boldsymbol{\sigma\nabla}) \\ i(\partial_0 - \boldsymbol{\sigma\nabla}) & -m \end{pmatrix} \begin{pmatrix} \phi_L(p) \\ \chi_R(p) \end{pmatrix} = 0. \tag{3.5.1}$$

decouples into the two Weyl equations

$$i(\partial_0 - \boldsymbol{\sigma\nabla})\phi_L(p) = 0 \tag{3.5.2}$$
$$i(\partial_0 + \boldsymbol{\sigma\nabla})\chi_R(p) = 0. \tag{3.5.3}$$

For a plane-wave we have that

$$\chi_R(p) = \chi_R \mathrm{e}^{-i\epsilon px} \quad \text{and} \quad p^0 = |\boldsymbol{p}| = E, \tag{3.5.4}$$

so for the limit $m = 0$ we get

$$(E - \boldsymbol{\sigma p})\chi_R \mathrm{e}^{-i\epsilon px} = 0. \tag{3.5.5}$$

Only the solution with positive helicity is allowed for a right-chiral Weyl fermion, since the dispersion relation is $E = \pm|\boldsymbol{p}|$ for both energy solutions $\epsilon = \pm 1$. Helicity is frame independent for a massless particle, so that right chirality (resp. left chirality) matches with positive helicity (resp. negative helicity) and we can call these particles right-handed (resp. left-handed). Therefore, Weyl fermions have two degrees of freedom: a left-handed 2-spinor with negative helicity and a right-handed 2-spinor with positive helicity.

Neutrinos were included in the SM as Weyl fermions and their conserved U(1) current was the lepton number L_l for the three flavors, so that the difference in number of leptons and anti-leptons of each family was conserved. However, neutrino oscillations mix the flavors so that only the total lepton number is conserved. This is caused by massive neutrinos only, so the discovery of neutrino oscillations is a sufficient condition to discard neutrinos as Weyl fermions.

Now we will focus on massive neutral fermions, called **Majorana fermions**. The Dirac field has to be complex due to group transformations that we will not discuss here, but a neutral field ψ_M only has half the degrees of freedom as a charged particle because we cannot distinguish particles from anti-particles. We can achieve that by using a self-conjugated field $\psi^c = \psi$,

$$\psi_{M,1} = \frac{1}{\sqrt{2}}(\psi_D + \psi_D^c) \tag{3.5.6}$$

$$\psi_{M,2} = \frac{1}{\sqrt{2}}(\psi_D - \psi_D^c), \tag{3.5.7}$$

in terms of the Dirac field, whereas in terms of Weyl spinors it is only composed of one 2-spinor and it conjugated

$$\psi_M^c = \psi_M = \begin{pmatrix} \phi_L \\ -i\sigma^2\phi_L^* \end{pmatrix}. \tag{3.5.8}$$

A Majorana fermion has therefore two degrees of freedom as well: one left-handed and one right-handed 2-spinor with both positive and negative helicities each.

A Dirac mass term connects the left-handed and righ-handed component of the same field and $\psi = \psi_L + \psi_R$ is a mass eigenstate. Therefore, if we define

$$\psi_L^c \equiv (\psi_L)^c = \frac{1}{2}(1+\gamma^5)\psi^c = (\psi^c)_R \tag{3.5.9}$$

we can obtain new Majorana mass terms as

$$-\mathscr{L}_L = m_L(\bar{\psi}_L^c\psi_L + \bar{\psi}_L\psi_L^c) \tag{3.5.10}$$

$$-\mathscr{L}_R = m_R(\bar{\psi}_R^c\psi_R + \bar{\psi}_R\psi_R^c), \tag{3.5.11}$$

or in terms of the new mass eigenstates

$$\mathscr{L}_L = -m_L\bar{\chi}\chi \tag{3.5.12}$$

$$\mathscr{L}_R = -m_R\bar{\omega}\omega, \tag{3.5.13}$$

where $\chi = \psi_L + \psi_L^c = \chi^c$ and $\omega = \psi_R + \psi_R^c = \omega^c$.

A general mass term icluding Dirac and Majorana fields reads as

$$-\mathscr{L}_{DM} = m_D\bar{\psi}_L\psi_R + m_L\bar{\psi}_L^c\psi_L + m_R\bar{\psi}_R^c\psi_R + h.c. \tag{3.5.14}$$

$$= \frac{1}{2}m_D(\bar{\chi}\omega + \bar{\omega}\chi) + m_L\bar{\chi}\chi + m_R\bar{\omega}\omega. \tag{3.5.15}$$

In order to have physical states with definite mass, we have to diagonalise the matrix

$$-\mathscr{L}_{DM} = \begin{pmatrix} \bar{\chi}, & \omega \end{pmatrix} \begin{pmatrix} m_L & \frac{m_D}{2} \\ \frac{m_D}{2} & m_R \end{pmatrix} \begin{pmatrix} \chi \\ \omega \end{pmatrix}, \tag{3.5.16}$$

so we find the eigenvalues

$$m_{1,2} = \frac{1}{2}\left\{(m_L + m_R) \pm \sqrt{(m_L - m_R)^2 + m_D^2}\right\}. \tag{3.5.17}$$

We cannot identify m_L in a gauge invariant way with the vev of the Higgs field, so Majorana mass terms of the type $m_L(\bar{\psi}_L^c \psi_L + \bar{\psi}_L \psi_L^c)$ for neutrinos do not appear in the SM. Experimental detection of violation of lepton number as in neutrinoless double β-decay would be a good proof of physics beyond the SM, but up to now it has not been found.

Before concluding this section, it is worth mentioning the *seessaw model*. Assuming that there exist left- and right-handed neutrinos, this model tries to explain why their masses are so much smaller than those of the other fermions in the SM . The right-handed ν_R is not affected by SM interactions and its mass will be taken to a value close to the cut-off scale used just like a scalar particle. Therefore, the eigenvalues in Eq. (3.5.17) become for $m_R \gg m_D$

$$m_1 \approx \tfrac{m_D^2}{2m_R} \quad \text{and} \quad m_2 \approx m_R. \tag{3.5.18}$$

For $m_R \sim 10^{14}$ GeV and $m_D \sim 100$ GeV we find light neutrino masses in the range of eV, which agrees with observations.

Chapter 4

Neutrino astronomy

Neutrinos are the most elusive elementary particles and their experimental study requires advanced techniques and technology. Previously we have focused on the theoretical description of neutrinos and throughout this Chapter we will try to provide a picture of the current observation methods and the motivations to invest such an effort on this quest. The last Section of this Chapter is devoted to the largest and most sensitive neutrino telescope ever made, IceCube, which is our only eye to see high-energy neutrinos.

4.1 Astrophysical sources of high-energy neutrinos

High-energy neutrinos are considered in the range $E_\nu \geq$ TeV. If we were able to detect their arrival directions with precision, they would directly point to their sources due to the little or no interaction during their cosmic trip. The only sources capable of producing such an energy are the so-called *cosmic accelerators*, primarily Supernovas (SN) and Active Galactic Nuclei (AGN). These high-energy neutrinos are very interesting to study because the range of energies allows us to get rid of most of the background noise at the detectors, that lies in the range of MeV for solar and up to TeV for atmospheric neutrinos. Most galactic sources are result of SN type II and their remnants (SNR), while almost all extragalactic sources are due to AGNs [36].

SN Type II or core collapse supernovae occur at the end of the fusion process in very massive stars, 8-20 solar masses. After the core is completely fused to iron, no further processes releasing energy are possible. Instead, photodisintegration destroys the heavy nuclei via $\gamma + {}^{56}\text{Fe} \rightarrow {}^{4}\text{He} + 4n$, and removes the thermal energy necessary to provide pressure support. In the following collapse of the star, the density increases and the free electrons are forced together with protons to form neutrons via inverse β-decay, emitting around 99% of the total SN energy. When the core density reaches nuclear density, the collapsing material rebounds and a shock wave propagates outwards heated by neutrino emission from the neutron star.

Pulsars may be good candidates for high-energy neutrinos, specially if they are part of a binary system. These objects are rapidly rotating neutron stars with a mass in the range 1.4-3 solar masses as the result of the SN II explosions. If the mass of the companion is large enough, the pulsar will orbit around it, since the center of mass of the system would be inside the companion. Pulsars have an intense magnetic field that can accelerate particles to very high energies. Protons for example will collide with the gas

of the outer layers of the companion's atmosphere and produce pions. Neutral pions will decay into pairs of photons that would allow us to detect the source through telescopes, whereas charged pions will decay through the process described in Sec. 3.2.1 to produce energetic muon neutrinos, which will be detected as muons after another charged weak interaction following the direction of the incoming neutrino.

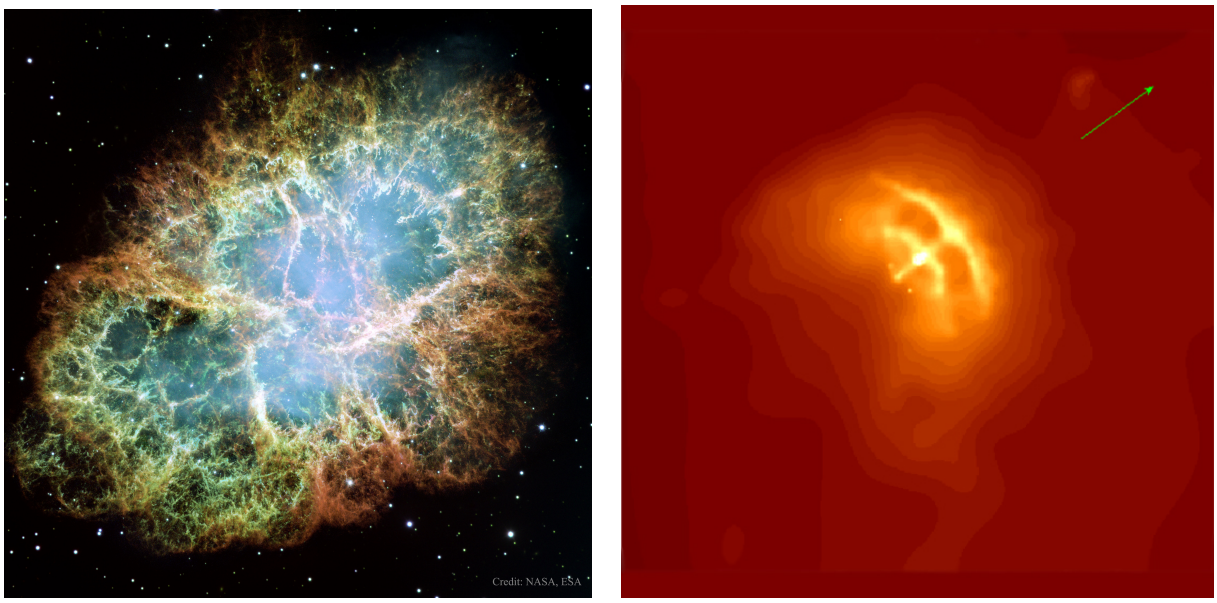

(a) (b)

Figure 4.1: Two examples of Supernova Remnants. Left: M1, the Crab Nebula from Hubble. Credit: NASA, ESA, J. Hester, A. Loll (ASU). Right: Vela Pulsar, a neutron star with rings and jet. Image from Chandra X-ray Observatory. The arrow indicates that the neutron star is moving along the direction of the x-ray jet. Credit: G.Garmire et al. (PSU), NASA.

AGN are compact regions at the centre of some galaxies that have a very high luminosity over most of the electromagnetic spectrum. The radiation from an AGN is believed to be a result of accretion of mass by a supermassive black hole at the centre of its host galaxy, where dissipative processes in the accretion disc transport matter inwards and angular momentum outwards, causing the accretion disc to heat up. Some accretion discs produce one or two collimated jets that emerge in opposite directions following the angular momentum axis of the accretion disc or the spin axis of the black hole. These relativistic particles may suffer scattering processes and produce secondary particles that would decay as described in Secs.3.2.1 and 3.2.2 to produce high-energy neutrinos. The standard model of AGN classifies them into two families, called radio-quiet and radio-loud. Radio-loud objects have emission contributions from both the jets and the lobes produced by them, which dominates the luminosity of the AGN at radio wavelengths. Examples of radio-loud AGN are radio galaxies, some quasars (quasi-stellar radio sources) and blazars (BL-Lac objects and OVV quasars). Radio-quiet objects are simpler since jet and any jet-related emission can be neglected at all wavelengths. Examples of this family are Seyfert 1 and Seyfert 2 galaxies as well as some other quasars. The above mentioned standard model of AGNs proposes that different observational classes of AGN are a single type of physical object observed under different conditions. The apparent differences between different types of objects arise because of their different orientation angle with respect to the observer, so that the quieter AGNs have their jets perpendicular

to the line of sight while the louder ones have them pointing towards the observer.

Within our galaxy we can find examples like the Crab Nebula (Fig.4.1a), or the Vela Supernova Remnant (Fig.4.1b). Extragalactic examples worth mentioning are the jet from M87 (Fig.4.2a) and distant quasars (Fig.4.2b).

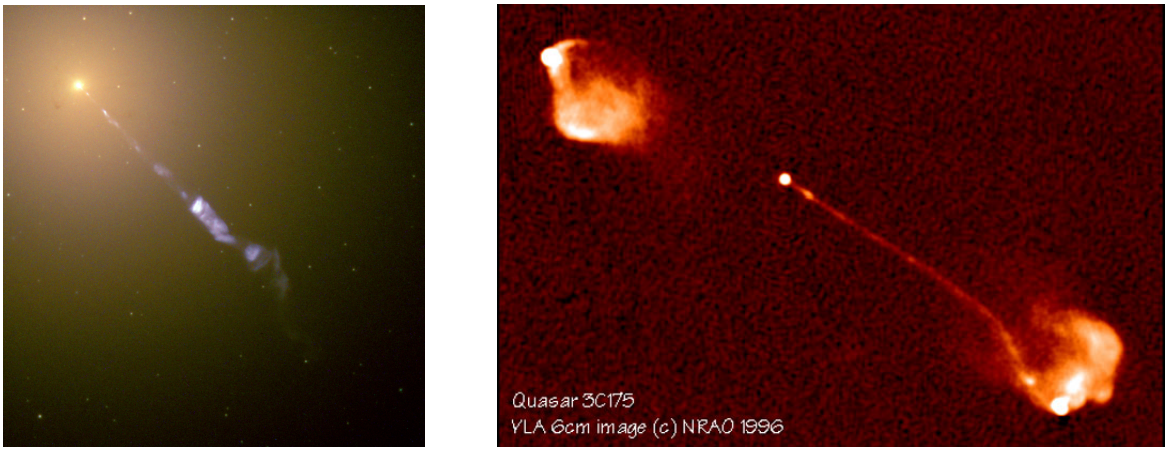

(a) (b)

Figure 4.2: Two examples of AGN. Left: A Jet from Galaxy M87, created by energetic gas swirling around a massive black hole at the galaxy's center. The jet is 5000 light-year long, where electrons are ejected outward at near light-speed, emitting blue light during a magnetic spiral. The dots of light surrounding M87's center are large ancient globular clusters of stars. Credit: J. A. Biretta et al., Hubble Heritage Team (STScI /AURA), NASA. Right: 3C175, a Quasar Cannon. The central dot is quasar 3C175. Image recorded by the Very Large Array (VLA) radiotelescopes. Shooting out from 3C175 is a thin jet of protons and electrons traveling near the speed of light that is over one million light-years long. Credit: Alan Bridle (NRAO Charlottesville) VLA, NRAO, NSF.

4.2 Cherenkov light

Neutrinos are not observed directly, but when they happen to interact with the ice they produce electrically charged secondary particles that in turn emit Cherenkov light, as a result of traveling through the ice faster than light travels in ice. The IceCube sensors collect this light, which is subsequently digitized and time stamped. This information is sent to computers in the IceCube Lab on the surface, which converts the messages from individual DOMs into light patterns that reveal the direction and energy of muons and neutrinos. Let us now cover the basics of Cherenkov radiation.

Cherenkov radiation is a well-understood phenomenon related to the passage of charged, ultra relativistic particles through a dielectric medium, discovered by P. A. Čerenkov in 1934 [38]. When a charged particle is moving through a medium faster than the speed of light in that medium, it causes the atoms in the medium to radiate. This radiation is caused by the sudden change in the value of the electric field surrounding the atom as the partice passes by. This radiation is emitted in the shape of a cone with axis in the

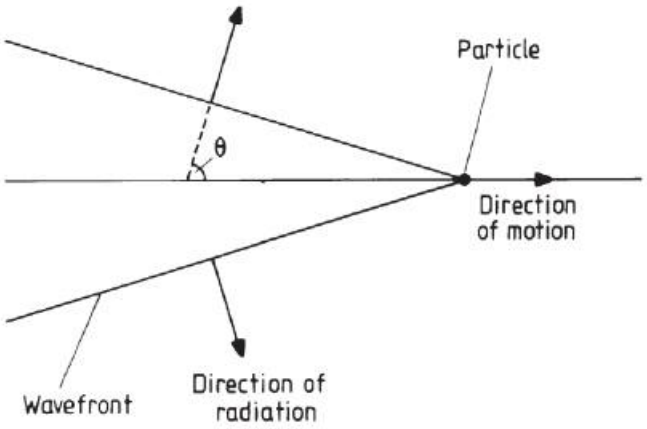

Figure 4.3: Cherenkov radiation of a particle moving through a medium without dispersion. The half-angle θ is formed by the direction of motion and the normal to the direction of radiation.[37]

direction of movement of the particle (Fig.4.3). The half-angle θ of this cone is

$$\cos\theta = \frac{1}{\beta \cdot n}, \tag{4.2.1}$$

where n is the refractive index of the medium and β is the relation between the speed of light in the vacuum c and the velocity of the particle v (where $v > c/n$).

Its spectrum is given by the Frank-Tamm formula

$$I_\nu = \frac{e^2\nu}{2}\left(1 - \frac{1}{n_\nu^2 v^2}\right), \tag{4.2.2}$$

where I_ν is the energy radiated at frequency ν per unit frequency interval, per unit distance travelled by the particle and e is the electric charge of the electron. This is the characteristic glow observed in the core of nuclear reactors (Fig.4.4).

The ice in Antarctica is not isotropic, but consists of hexagonal crystals that are oriented in the same direction [39, 40]. This orientation leads to an anisotropy, and the Cherenkov radiation may depend on the direction of the ice orientation. This is of particular interest because IceCube has already observed an anistropy in the ice, believed to be due to the scattering depending on the azimuthal direction the photon follows through the medium [41]. A theory of Cherenkov radiation in a uniaxial medium could be required [42]. In anisotropic media, optical Cherenkov emission depends on the angle between the relativistic charged particle and the optical axis of the medium. In oriented ice crystals, the Cherenkov emission rate varies slightly, by 0.3%, and the emission angle can vary by 0.4 degrees [43]. However, this results indicate that experiments like IceCube can safely neglect the effect of crystal anisotropy in their data analysis.

4.3 Detecting neutrinos

The first dedicated neutrino oscillation experiment started operating in 1968 under the direction of Ray Davis Jr and his group [18] and was based on the *chlorine* − 37 technique. It was designed to detect electron neutrinos from the Sun with a threshold

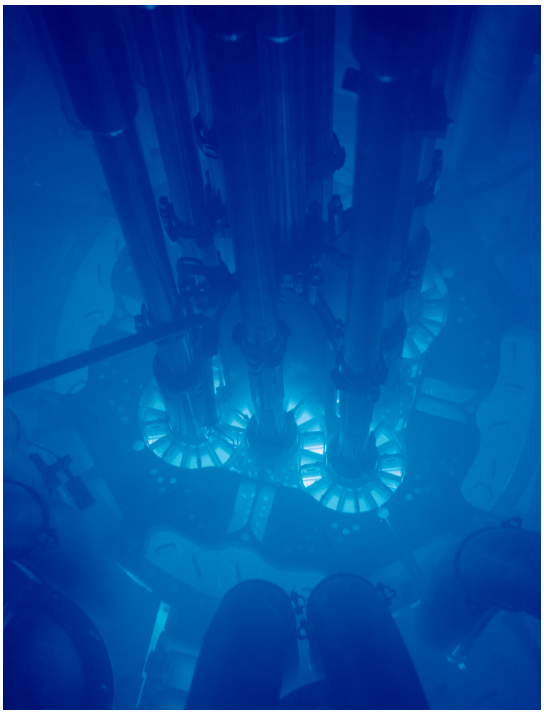

Figure 4.4: Cherenkov radiation glowing in the core of the Advanced Test Reactor. By Argonne National Laboratory, Idaho National Laboratory, USA.

energy of 0.814MeV using the reaction

$$\nu + {}^{37}_{17}\mathrm{Cl} \rightarrow {}^{37}_{18}\mathrm{Ar} + e^{-}. \tag{4.3.1}$$

The interaction of a neutrino with the chlorine isotope produces a radioactive isotope of argon, which decays back to the same chlorine by capturing one of its own inner orbital electrons while ejecting another one with a 2.8 keV energy. These emited electrons are counted as a measure of the number of argon iotopes produced by neutrino interactions. The detection rate was 2.23 $\pm$ 0.22 SNU. The solar neutrino unit, SNU, corresponds to 10^{-36} captures per second per target atom. The expected rate from the Sun is 7.3 $\pm$ 1.5 SNU and this disparity led to the solar neutrino problem before neutrino oscillations were discovered. Davis shared the Nobel prize for physics in 2002 for his work.

The next generation of neutrino detectors were water-based and their primary objective was proton decay detection and not neutrinos [16]. The principle is Cherenkov radiation form the products of neutrino interactions, namely electron scattering and inverse β-decay. A high-energy neutrino of any flavor interacts with an electron and transfers its energy, shooting the electron with a speed larger that the speed of light in water and approximately in the same direction. On the other hand, in inverse β-decay, an energetic positron is produced as described by Eq. (2.2.4). Both the positron and electron traveling through water produce Cherenkov radiation in a cone around the direction of motion, which is collected by photomultipliers. This radiation can be used to calculate the energy of the incoming neutrino and the direction of arrival in case of a scattering event.

The muon neutrino interacts with a proton to produce a relativistic muon (see Eq. (2.2.8)). The Cherenkov radiation of this muon leaves a characteristic ring of light, that contrasts with the blurry ring left by the electron neutrino scattering due to the γ-ray pairs

produced by the outgoing electron that create electron-positron pairs that also produce Cherenkov light. SuperKamiokande was able to detect them and thus provided evidence for neutrino oscillations in 1998. Due to pion decay after atmospheric interaction of cosmic rays, there should be twice as many muon-neutrinos as electron-neutrinos (Eq. (2.2.9)). However, SuperKamiokande found that this was true for neutrinos coming directly from above but that the number of neutrinos of both flavors coming from the other side of the Earth was roughly the same. The only explanation was that half of the muon-neutrinos must have oscillated into tau-neutrinos. This was confirmed in 2000 by a 30% shortage of the detected muon-neutrinos from the artificial source at the KEK laboratory at Tsukuba [19].

This leads to our main interest, IceCube. This detector is located under more than one kilometer of Antarctic ice, which is highly transparent due to the few impurities and the pressure that has pushed out any air bubble. Therefore, Cherenkov radiation can be easily detected by the photomultipliers.

4.4 IceCube experiment

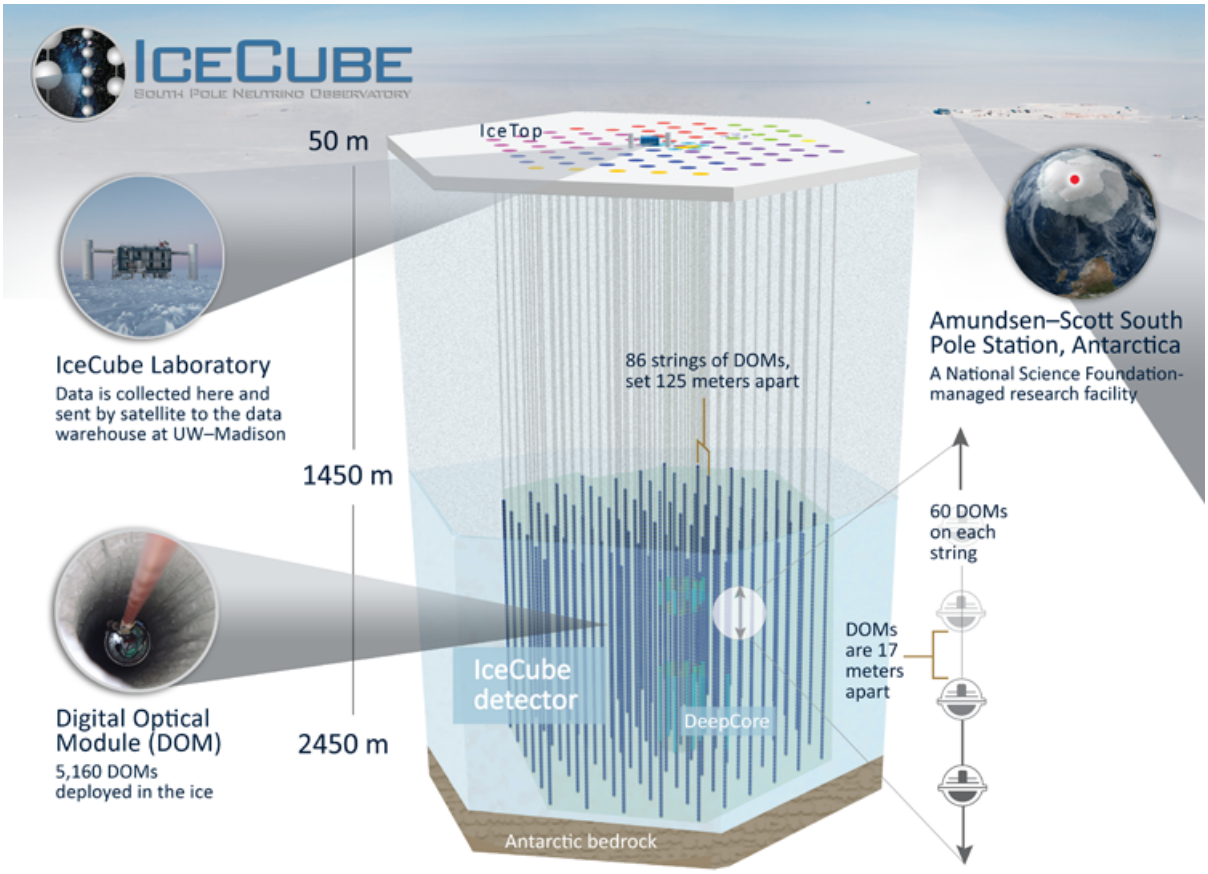

Figure 4.5: Design of the IceCube detector at the Amundsen-Scott base in Antarctica. Copyright: IceCube Collaboration. [44]

IceCube, the South Pole neutrino observatory, is a cubic-kilometer particle detector made of Antarctic ice and located near the Amundsen-Scott South Pole Station. It is

buried beneath the surface, extending to a depth of about 2,500 meters. A surface array, IceTop, and a denser inner subdetector, DeepCore, significantly enhance the capabilities of the observatory, making it a multipurpose facility [44].

As seen in Fig.4.5, the in-ice component of IceCube consists of 5,160 digital optical modules (DOMs), each with a ten-inch photomultiplier tube and associated electronics. The DOMs are attached to vertical strings in 86 holes, and displayed over a cubic-kilometer from 1,450 meters to 2,450 meters depth. Each string holds 60 DOMs separated 17 meters and they are deployed on a hexagonal grid with 125 meters spacing.

Eight of these strings at the center of the array were deployed more compactly, with a horizontal separation of about 70 meters and a vertical DOM spacing of 7 meters. This denser configuration forms the DeepCore subdetector, which lowers the neutrino energy threshold to about 10 GeV, creating the opportunity to study neutrino oscillations and perform searches for *sterile neutrinos*.

IceTop consists of 81 stations located on top of the same number of IceCube strings. Each station has two tanks, each equipped with two downward facing DOMs. IceTop also detects air showers from primary cosmic rays in the 300 TeV to 1 EeV energy range. The surface array measures the cosmic-ray arrival directions in the Southern Hemisphere as well as the flux and composition of cosmic rays.

IceCube was built to search for very high energy neutrinos created in the most extreme cosmic environments. The improved performance at EeV energies has opened a window to search for cosmogenic neutrino interactions, produced by the interaction of extragalactic cosmic rays with photons of the cosmic microwave background (CMB).

IceCube has observed the first astrophysical high-energy neutrino flux ever, with significance at the 5.7 σ level after analyzing three years of data (2010-2013) [45]. In this search, they discovered three neutrino events with energies at the PeV level. These are the highest energy neutrinos ever detected, shown in Fig. 4.6.

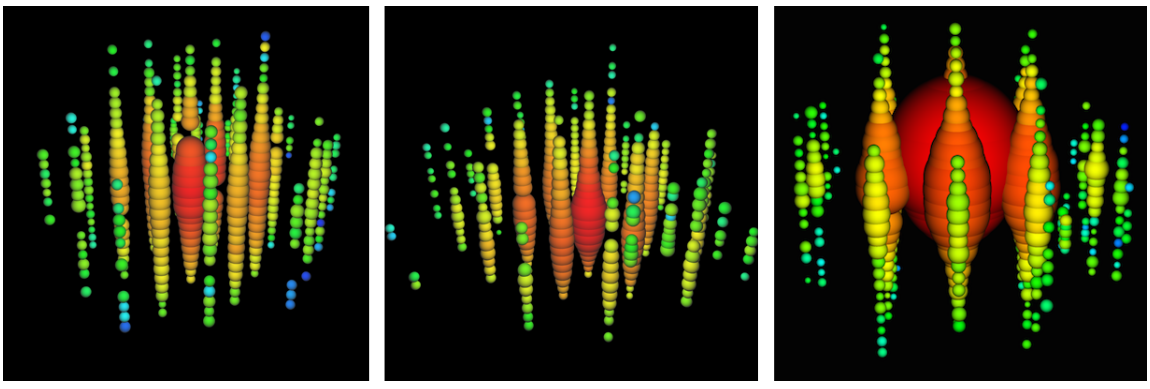

Figure 4.6: IceCube has detected the highest energy neutrinos ever recorded, with energies reaching above 2 PeV. From left to right, Bert, Ernie and Big Bird, with energies of 1.0, 1.1 and 2.2 PeV.

Chapter 5

Flavor oscillations as detected on Earth

After discussing the theoretical and experimental properties of neutrinos, it is time to try to apply them to the specific case of the high-energy flux range. We will focus on two specific models, as mentioned in previous Sections: vacuum oscillations and MSW effect in presence of a DM halo in the Milky Way. For that purpose, we have collected some of the latest publications on the topic and designed simple computer simulations using C++ [46]. For the vacuum model we apply the three-flavor theory but for the oscillations in DM model we follow the literature on the MSW effect and apply the two-flavor approximation.

5.1 Tribimaximal expectation

As an introductory section, we will try to reproduce the tribimaximal expectation of neutrino flavors as we would detect it. Decoherence of the flavor ratio occurs during propagation over cosmic distances, so that oscillations are averaged and the detection ratio is expected to be $(1:1:1)_\oplus$ [47]. We can calculate the expected flavor ratio from any source ratio using Eq. (2.4.11),

$$\{\alpha_{j,\oplus}\} = \sum_{k,i} |U_{jk}|^2 |U_{ik}|^2 \{\alpha_{i,S}\}, \tag{5.1.1}$$

where $\{\alpha_i\}$ is a vector whose components are the ratios of the three neutrino flavors $i = e,\ \mu,\ \tau$. The index $\oplus$ stands for *Earth*, S stands for *source* and $U_{\mu\nu}$ are the componens of the neutrino mixing matrix (Eq. (2.4.12)).

We calculate the expected neutrino ratio on Earth using the mixing angles and the CP-phase presented in Table 2.1 for a fixed source ratio $\{\alpha_{i,S}\} = (1:2:0)_S$. Those parameters are given as a range, so we will use here three U matrices: one for the average value of the angles, one for the maximum value and one for the minimum, always imposing the unitarity condition. We then present our results in a double table to compare the two disconnected ranges of θ_{23}. These correspond to the normal and inverted mass hierarchies (left and right panels respectively).

The results presented in Table 5.1 through the simulation are not far from the tribimaximal expectation $(1:1:1)_\oplus$. We observe that the best relation for us is obtained for

Table 5.1: Neutrino flavor ratio on Earth for different values of the mixing angles and CP-phase in the 3σ range [25]. The disconnected ranges of θ_{23} are separately presented in two tables: the left one for the normal mass hierarchy and the right one for the hierarchy. The first row corresponds to the best fit parameters, the second row is the maximum of the 3σ range, while the last row is the minimum.

Input (°)	$\{\alpha_{i,\oplus}\}$
$\theta_{12} = 33.36$ $\theta_{23} = 40.00$ $\theta_{12} = 8.66$ $\delta_{CP} = 300.00$	$(1.0918 : 0.9767 : 1.1131)_\oplus$
$\theta_{12} = 34.17$ $\theta_{23} = 42.10$ $\theta_{12} = 9.10$ $\delta_{CP} = 366.00$	$(1.0910 : 0.9777 : 1.0298)_\oplus$
$\theta_{12} = 32.58$ $\theta_{23} = 38.50$ $\theta_{12} = 8.20$ $\delta_{CP} = 162.00$	$(1.0342 : 1.0475 : 1.1790)_\oplus$

Input (°)	$\{\alpha_{i,\oplus}\}$
$\theta_{12} = 33.36$ $\theta_{23} = 50.40$ $\theta_{12} = 8.66$ $\delta_{CP} = 300.00$	$(0.9555 : 1.0585 : 0.8275)_\oplus$
$\theta_{12} = 34.17$ $\theta_{23} = 51.70$ $\theta_{12} = 9.10$ $\delta_{CP} = 366.00$	$(0.9548 : 1.0903 : 0.7684)_\oplus$
$\theta_{12} = 32.58$ $\theta_{23} = 49.10$ $\theta_{12} = 8.20$ $\delta_{CP} = 162.00$	$(0.8968 : 1.0745 : 0.8930)_\oplus$

the maximal values of the mixing angles in the lower range of θ_{23}.

The tribimaximal expectation is however disfavoured at 79% confidence level by statistical analysis of the IceCube data [48].

5.2 Vacuum oscillations at IceCube

In this section we will try to explore the flavor composition of neutrinos as detected by IceCube focusing on *High Energy Starting Events* (HESE). The first issue is to discriminate between *shower* and *track* events. This is a purely topological classification of events in a detector that allows us to identify their nature. Showers are caused by neutral current (NC) interactions of all neutrino flavors and charged current (CC) interactions of ν_e and ν_τ (Fig. 5.1a), while tracks are the result of CC interactions of ν_μ (Fig. 5.1b).

Using the description of the IceCube detector published by the Collaboration [45] we can calculate the expected number of events of neutrinos and antineutrinos as,

$$N = 4\pi T \int \mathrm{d}E \; \Phi_l(E) A_l(E), \tag{5.2.1}$$

where l stands for the lepton flavor $l = e, \mu, \tau$, Φ is an isotropic flux, T is the observation time and $A_l(E)$ is the energy-dependent effective area of the detector, that include the effects of neutrino cross sections, partial neutrino absorption in the Earth, detector efficiency and specific cuts of the HESE analysis.

To calculate the track-to-shower ratio we separate contributions to the effective areas and calculate the number of tracks and showers separately as,

$$N_S = 4\pi T \int_{\bar{E}_0}^{\bar{E}} \mathrm{d}E \; \{\Phi_e(E) A_e(E) + \Phi_\tau(E) A_\tau(E) + \Phi_\mu(E)[1 - p_T] A_\mu(E)\}, \tag{5.2.2}$$

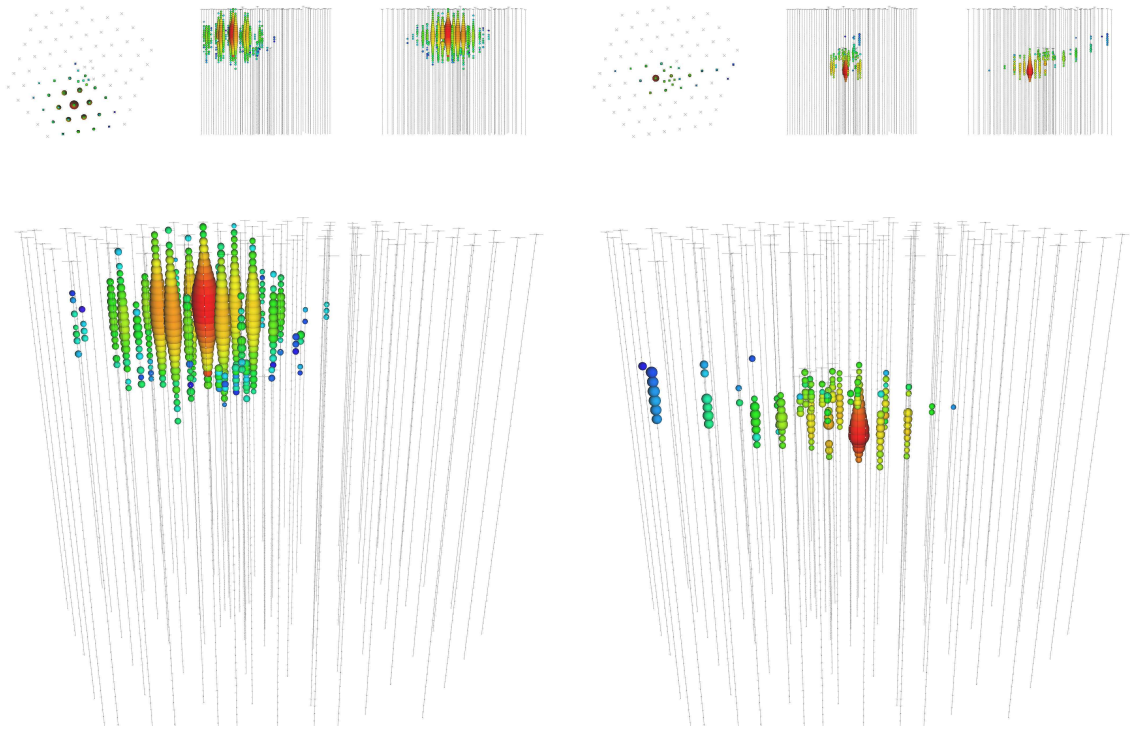

(a) (b)

Figure 5.1: Comparison between a shower and a track event in IceCube [45]. 5.1a- Shower event of 2 PeV. Most energetic event registered by IceCube. 5.1b- Track event of 30.8 TeV.

and

$$N_T = 4\pi T \int_{\bar{E}_0}^{\bar{E}} \mathrm{d}E \; \Phi_\mu(E) p_T A_\mu(E), \tag{5.2.3}$$

where p_T is the probability that an observed event produced by a muon neutrino is a track event. It depends mildly on the neutrino energy and its value is approximately 0.8 [49]. The integration limits are chosen based on the purposes of this work. We are focusing on high-energy neutrinos and therefore we start the calculations with a lower limit $\bar{E}_0$ of 60 TeV. The cut-off energy $\bar{E}$ is chosen to be 3 PeV because the most energetic event detected is in the neighbourhood of 2 PeV [45]. Cosmic neutrinos have been detected isotropically, so their fluxes can be averaged over the directions and expressed by a power law distribution up to a maximum value,

$$\Phi_l(E) = \frac{F_l \cdot 10^{-8}}{\mathrm{cm}^2 \ \mathrm{s} \ \mathrm{sr} \ \mathrm{GeV}} \left(\frac{\mathrm{GeV}}{E} \right)^2, \tag{5.2.4}$$

where F_l are adimensional non-negative coefficients for each neutrino flavor and α is the spectral index that we chose to be 2, in agreement with experimental data [49]. Integrating numerically we find the values

$$N_S = 8.398 \times F_e + 0.976 \times F_\mu + 6.504 \times F_\tau \tag{5.2.5}$$

$$N_T = 3.907 \times F_\mu. \tag{5.2.6}$$

The track-to-shower ratio can then be calculated as

$$\frac{N_T}{N_S} = \frac{3.907 \times F_\mu}{8.398 \times F_e + 0.976 \times F_\mu + 6.504 \times F_\tau}. \tag{5.2.7}$$

Inserting the tribimaximal expectation in this equation we find the value,

$$\left(\frac{N_T}{N_S}\right)_{\oplus} = 0.246. \tag{5.2.8}$$

However, this hypothesis has been discarded after IceCube data and so we have to go into further analysis. Using the calculations from Sections 2.4 and 5.1-5.2 and data from [25] we perfom a Monte Carlo simulation of the neutrino flavor oscillations using Eq. (5.1.1) including the margin of error for the measurements of the mixing angles and the CP-phase. We then insert these flavor ranges in Eq. (5.2.7) to obtain a more realistic distribution and explore some predictions for future upgrades of IceCube.

We present in Fig. 5.2 the expected track-to-shower ratio on Earth for the simulation of 20.000 high-energy neutrinos in the range 60-3000 TeV generated by four different mechanisms:

1. Charmed meson decay (1/2:1/2:0) in purple.
2. π decay (1/3:2/3:0) in green.
3. β-decay of neutrons (1:0:0) in light blue.
4. π decay with damped muons (0:1:0) in dark yellow.

We can see that the track-to-shower ratio corresponding to the tribimaximal approximation is favoured for neutrinos generated via decay of pions with damped muons, while it is comletely excluded for neutrinos coming from neutron decay. It is marginally compatible with neutrinos generated by mesons.

Evaluating the data from IceCube we could add a distribution to that graph to compare the ranges and areas of the expected and detected ratios and thus exclude some regions and obtain information about the sources of neutrinos. Between the years 2010 and 2014, IceCube has detected a total number of $n_T = 8$ tracks and $n_S = 24$ showers [45, 50]. This is, however, not enough data to provide statistical information about exclusion regions or to establish constraints on the production mechanisms. It will be interesting to observe the results of more years of observations and compare them to this and other models.

5.3 Oscillations in a Dark Matter density profile

As a final section, we will explore a more exotic view of the Milky Way and how that affects neutrino oscillations. The latest observations by the Planck Collaboration [51] show that the abundance of Dark Matter (DM) is around 85% of the total amount of matter and 23% of the total energy of the Universe. The matter composition of galaxies is therefore dominated by DM and so neutrinos traveling across the Galaxy would be affected by its presence through the MSW mechanism mentioned in Sec. 2.5. Let us briefly justify the existence and importance of DM before proceeding [52, 53].

The need for DM comes from observational evidences. Rotation curves of galaxies in the 1970s were the first indicator that most of the matter in the Universe was non-baryonic. The motion of stars in galaxies was considered to follow the Kepler laws since

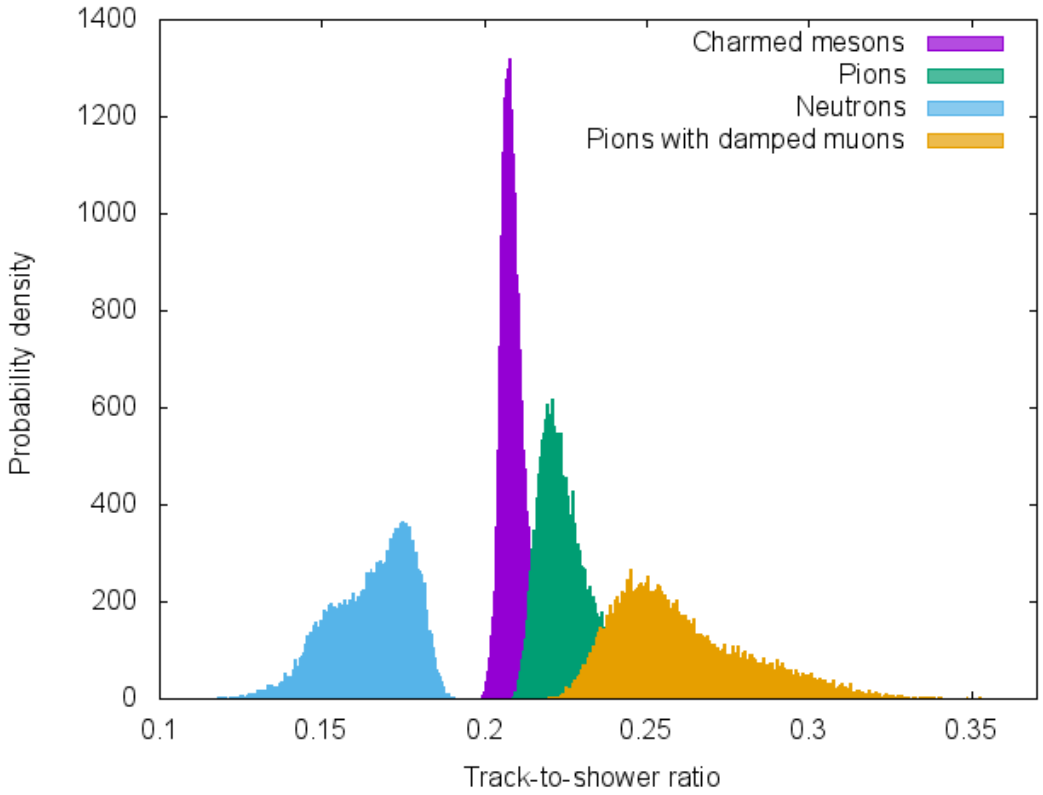

Figure 5.2: Track-to-shower ratios for the four known production mechanisms of neutrinos as expected on Earth. This result is given for 20,000 neutrinos sent from the source with the different relative abundances using an algorith that includes the cross sections and simulated detector parameters. This graph shows the dependance of the track-to-shower ratios on the uncertainties of the mixing angles.

the famous German mathematician formulated them to explain the orbits of the planets in the Solar System following Tycho Brahe's observations. The orbital velocity resulting from the equilibrium of the gravitational and centrifugal forces is

$$v = \sqrt{GM/r}, \tag{5.3.1}$$

where G is Newton's gravitational constant, M is the mass of the Sun and r is the radius of the orbit (Fig. 5.3a).

If we assume that the majority of a galaxy's mass is located near the center, we could expect a velocity distribution for the stars around the galaxy similar to the previous relation. However, the observed rotation velocities are almost constant for stars along the galactic disc outwards (Fig. 5.3b). This suggests that the majority of the mass is not situated in the nucleus of the galaxy but in the halo with a spherically simmetric density distribution $\rho \propto 1/r^2$. Also, this matter does not emit light in any range of the electromagnetic spectrum and therefore receives the name *"dark"*.

Another indirect evidence of the existence of DM is the enhancement of the *gravitational lensing* effect. Following the theory of General Relativity, the presence of large masses bend the trajectories of the photons as they travel through space. This hypothesis was proved through observtions of stars behind the Sun during a total eclipse in 1919 by

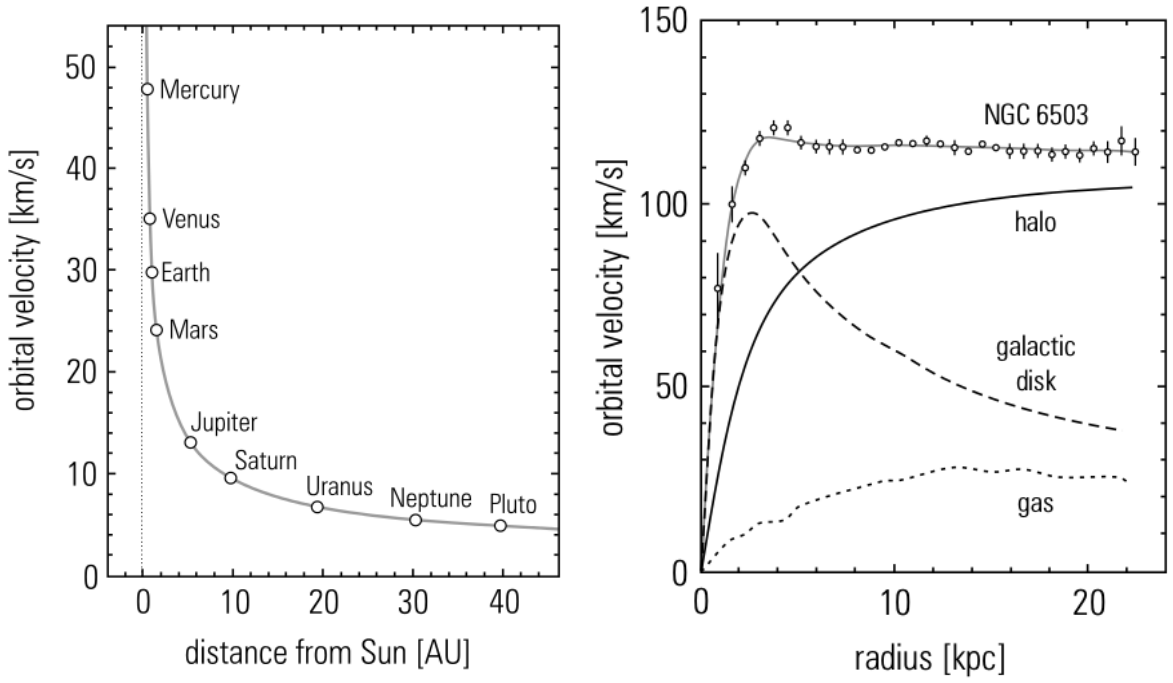

(a) (b)

Figure 5.3: Rotation curves for the planets of the Solar System as a function of the distance to the Sun (left) and for the stars, gas, disk and halo in the galaxy NGC 6503 as a function of the distance to the galactic center (right). Credit: [53].

Eddington [54]. This effect is highly increased at cosmic scale when a galaxy or cluster bends the light emitted by a further luminous object behind it (Fig. 5.4). A detailed analysis of this effect is beyond the scope of this work, but it is worth mentioning that mathematical derivations of the expected mass of these cosmic lenses do not match the observed luminous mass. This disagreement supports the idea of dark matter as the invisible contribution dominating gravity.

The matter in galaxy cluster 1E 0657-56, known as the "Bullet Cluster", is shown in Fig.5.5. Situated 3.4 billion light-years away, the cluster's individual galaxies are seen in the optical image data, but their total mass adds up to far less than the mass of the cluster's two clouds of hot x-ray emitting gas shown in red. Representing even more mass than the optical galaxies and x-ray gas combined, the blue hues show the distribution of dark matter in the cluster. Otherwise invisible to telescopic views, the dark matter was mapped by observations of gravitational lensing of background galaxies. The bullet-shaped cloud of gas at the right was distorted during the collision between two galaxy clusters that created the larger bullet cluster itself. But the dark matter present has not interacted with the cluster gas except by gravity. The clear separation of dark matter and gas clouds is considered a strong evidence that dark matter exists.

Neutrinos were considered a good candidate for DM particle, since they do not emit or absorb light and very rarely interact with ordinary matter. However, due to their low mass, the number density required to add up to the calculated masses of galaxies and clusters would too high. Another inconvenient is that neutrinos are ultrarrelativistic particles, which would prevent from the formation of large cosmic structures in the prim-

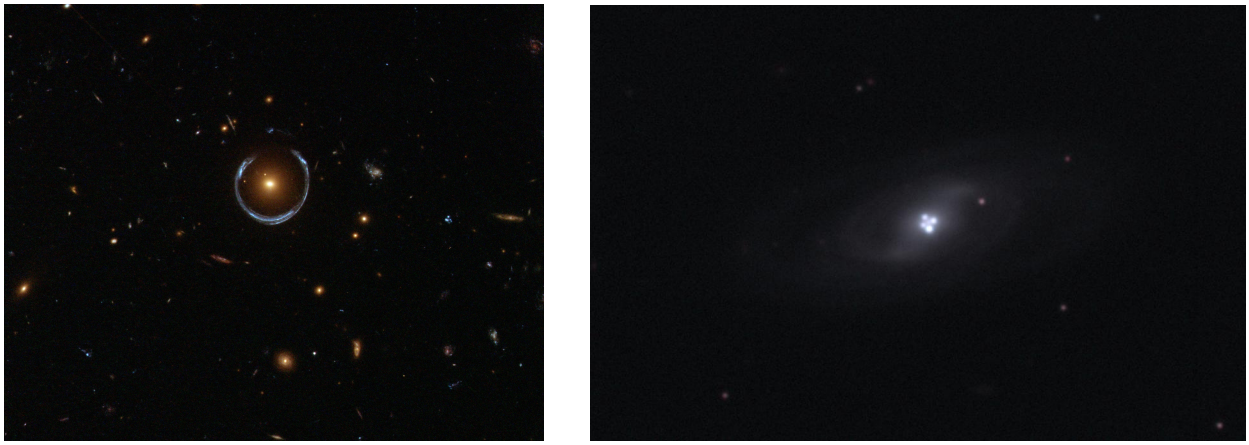

(a) (b)

Figure 5.4: Einstein ring (left) and Einstein cross (right). The massive galaxy in the center of each image bends and distorts the light from the object perfectly aligned behind it. Credit: ESA/Hubble & NASA (left), J. Rhoads (Arizona State U.) et al., WIYN, AURA, NOAO, NSF (right).

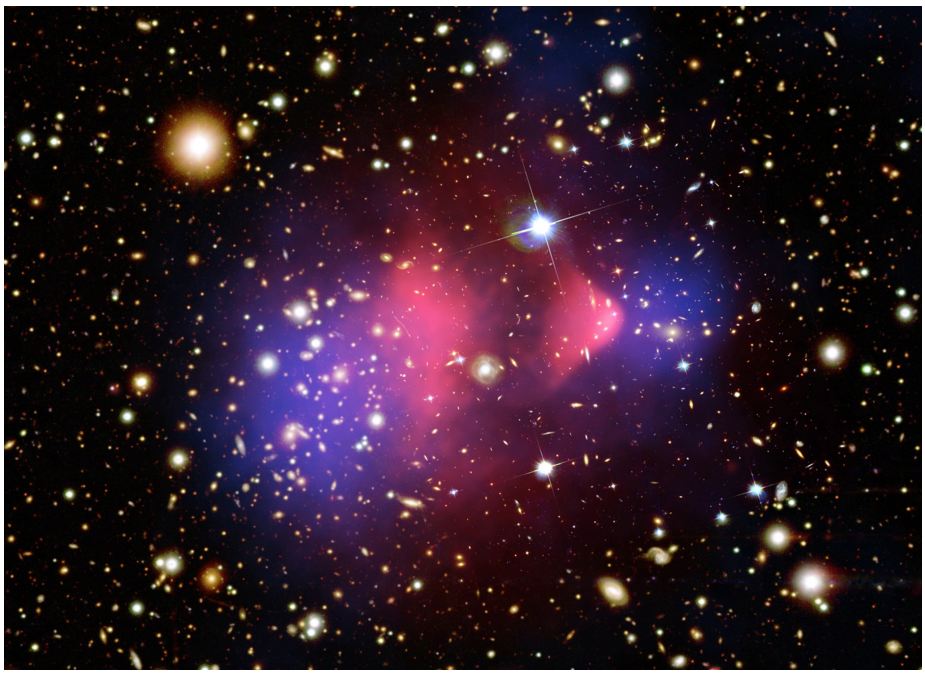

Figure 5.5: Bullet Cluster, 1E 0657-56. The luminous galaxies (visible) and the DM halo (false blue) continue without big interactions. The gas clouds (false red) are left behind after the collision. This is one of the strongest evidences of the existence of dark matter in the universe. Credit: NASA.

itive Universe. This *Hot Dark Matter* is considered a only small contribution to the total amount and current theories contemplate a picture dominated by *Cold Dark Matter* that would be more massive and subrelativistic.

Having said this, we can proceed to evaluate the effect of DM in the Milky Way on neutrino oscillations. We can assume a two-flavor oscillation scenario where ν_e change into the combination $\nu_a = (\nu_\mu + \nu_\tau)/\sqrt{2}$. Therefore, neutrino evolution is determined by four parameters: the mass-squared splitting Δm^2, the mixing angle θ, the neutrino energy E_ν and the number density of the DM particles in the medium N_χ.

We will follow the same reasoning as for the solar neutrinos [55, 56], including a spherically symmetric DM profile in the Galaxy intead of the infinite exponential profile [57],

$$\rho_{\rm DM}(r, r_s, \alpha, \beta, \gamma) = \rho_\oplus \left(\frac{r_\oplus}{r}\right)^\gamma \left(\frac{1 + (r_\oplus/r_s)^\alpha}{1 + (r/r_s)^\alpha}\right)^{(\beta-\gamma)/\alpha}, \tag{5.3.2}$$

where $r_\oplus = 8$ kpc is the distance of the Solar System to the Galactic Center (GC) $r = 0$ and $\rho_\oplus = 0.4$ GeV/cm^3 is the local DM energy density. We will focus in an *isothermal* DM profile [58],

$$\rho_{\rm iso}(r) = \rho_{\rm DM}(r, 5\ {\rm kpc}, 2, 2, 0), \tag{5.3.3}$$

that gives the distribution

$$\rho_{\rm iso}(r) = \frac{38.9}{r^2 + 25}\ ({\rm GeV/cm^3}), \tag{5.3.4}$$

as shown in Fig. 5.6.

We have to solve Schrödinger's equation

$$i\frac{{\rm d}\phi}{{\rm d}t} = H\phi, \tag{5.3.5}$$

where $\phi = (\phi_1, \phi_2)^T$ is the vector whose components are the two neutrino sates, labeling the heavier state as "2" so Δ_{m^2} is positive and θ is in the range $[0 : 2\pi]$. The hamiltonian is

$$H = \begin{pmatrix} i\Delta_m/(4E_\nu\theta'_m) & -1 \\ 1 & -i\Delta_m/(4E_\nu\theta'_m) \end{pmatrix}, \tag{5.3.6}$$

where

$$\Delta_m = \sqrt{(A - \Delta\cos 2\theta)^2 + (\Delta \sin 2\theta)^2} \tag{5.3.7}$$

is the effective mass difference between the neutrino states and θ_m is the mixing angle in matter expressed as

$$\tan 2\theta_m = \frac{\Delta \sin 2\theta}{A - \Delta\cos 2\theta}, \tag{5.3.8}$$

where we define $\Delta \equiv \Delta m^2/(4E_\nu)$.

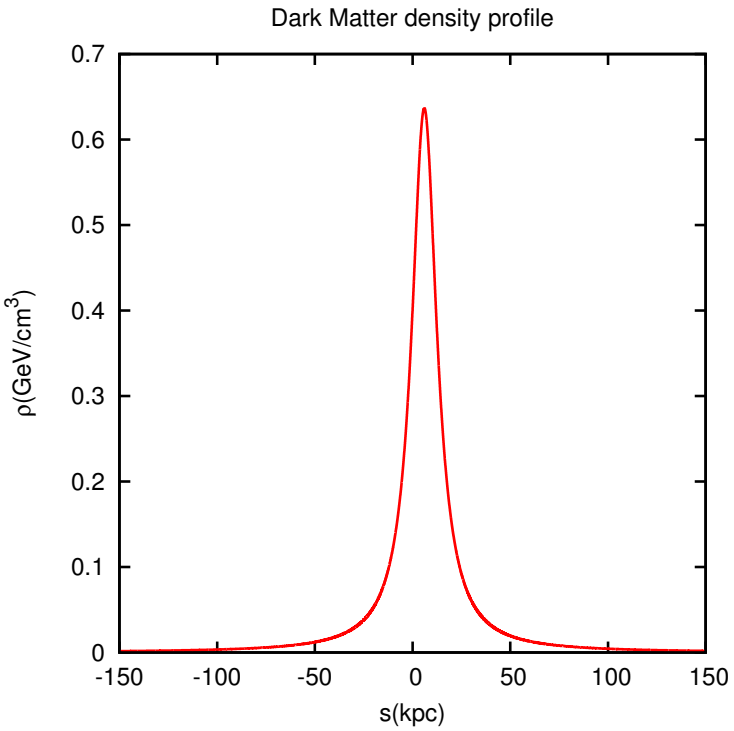

Figure 5.6: Dark matter density profile for the Milky Way as described by the isothermal model as a function of the line of sight in kpc.

We can rewrite Δ_m and θ'_m in terms of θ_m as

$$\theta'_m = \frac{\sin^2 2\theta_m}{2\Delta \sin 2\theta} \frac{\mathrm{d}A}{\mathrm{d}r}, \tag{5.3.9}$$

$$\frac{\Delta_m}{\theta'_m} = \frac{2\Delta^2 \sin^2 2\theta}{\sin^3 2\theta_m} \frac{1}{\mathrm{d}A/\mathrm{d}r}, \tag{5.3.10}$$

$$A = \frac{\Delta \sin(2\theta_m - 2\theta)}{\sin 2\theta_m}. \tag{5.3.11}$$

The effective potential describing the interaction between neutrinos and the DM particles can be expressed in the flavor basis as [57]

$$\mathcal{V}_{\alpha\beta} = \lambda_{\alpha\beta} G_F N_\chi, \tag{5.3.12}$$

where $\lambda_{\alpha\beta}$ is a hermitian matrix whose components are the effective couplings between DM and neutrinos, that we will consider to be real, $G_F = 1.16637 \cdot 10^{-5}$ GeV^{-2} is the Fermi constant and N_χ is the DM number density, expressed as

$$N_\chi = \frac{\rho_{\mathrm{DM}}}{m_{\mathrm{DM}}}. \tag{5.3.13}$$

Variations in the entries of the effective potential give similar results, so for simplicity we will consider the effective potential to be the scalar quantity

$$A = |\mathcal{V}_{\alpha\beta}| = V G_F \rho_{\mathrm{DM}}, \tag{5.3.14}$$

where we have defined $V = |\lambda_{\alpha\beta}|/m_{DM}$ (in GeV^{-1}) to take in consideration the two unknown parameters of the theory altogether.

For a numerical simulation of neutrino oscillations in the isothermal DM profile, we choose the Hamiltonian to be instantaneously diagonal throughout the whole process. Also, the Solar System is not situated at the center of the Galaxy, so we will define the *line of sight* distance s and the angle of observation ϕ so that the galactocengtric distance reads as

$$r^2 = s^2 + r_\oplus^2 - 2sr_\oplus \cos\phi. \tag{5.3.15}$$

We will evaluate this process for different values of the vacuum mixing angle θ, the observation angle ϕ and the effective potential V. Since we are considering high-energy neutrinos, we will fix $\Delta = 10^{-9}$ eV^2/GeV. In Figs. 5.7, 5.8 and 5.9 we present the effect of θ, ϕ and V over the probability of finding an electron neutrino or a non-electron neutrino as a function of the line of sight. For each figure, we keep two parameters fixed and vary the third one. The fourth plot in each figure shows how the mixing angle in matter is affected by those parameters.

The first remarkable aspect of each figure is the change of the slope of the probability curves around the GC, which coincides with the maximum value of the mixing angle in matter. This is related to the condition of adiabaticity, Eq. (2.5.7), that is maximally violated in this point (PMVA). The fast change of the mixing angle in matter enhances this effect, as better seen in Figs. 5.7c, 5.8c and 5.9a and their corresponding θ_m curves. The fast change in the density of the DM halo causes that neutrinos cannot keep the fast pace of the instantaneous eigenstates of the Hamiltonian (Eq. (5.3.6)) and the transitions $\nu_{1m} \leftrightarrow \nu_{2m}$ (that we had avoided up to now) are present. These then modify the probability of finding a flavour eigenstate in the non-adiabatic region affected by both the vacuum mixing angle and the potential.

The oscillation is barely affected by the direction of the incoming neutrino, as we observe in Fig. 5.7. The Earth is situated very close to the GC compared to the dimension of the DM halo and isotropy could be assumed. Only very small observation angles with respect to the GC provide some variations.

The vacuum mixing angle, on the other hand, affects drastically the behaviour of the oscillation, as seen in Fig. 5.8. Smaller mixing angles cause faster oscillations, while larger values tend to reduce them.

Finally, we observe in Fig. 5.9 that the potential varies the length scale of the oscillation, suppressing it for values lower than the squared mass difference as well as for values three orders of magnitude higher. The increase of V is equivalent to an increase of E_ν [57], so the effects of the DM profile would be more relevant to higher neutrino energies. This could therefore explain non-standard neutrino flavor composition for high-energy fluxes detected at IceCube, without contradicting lower-energy data. The variation of V can also be inferred to estimate the mass range of the DM particles.

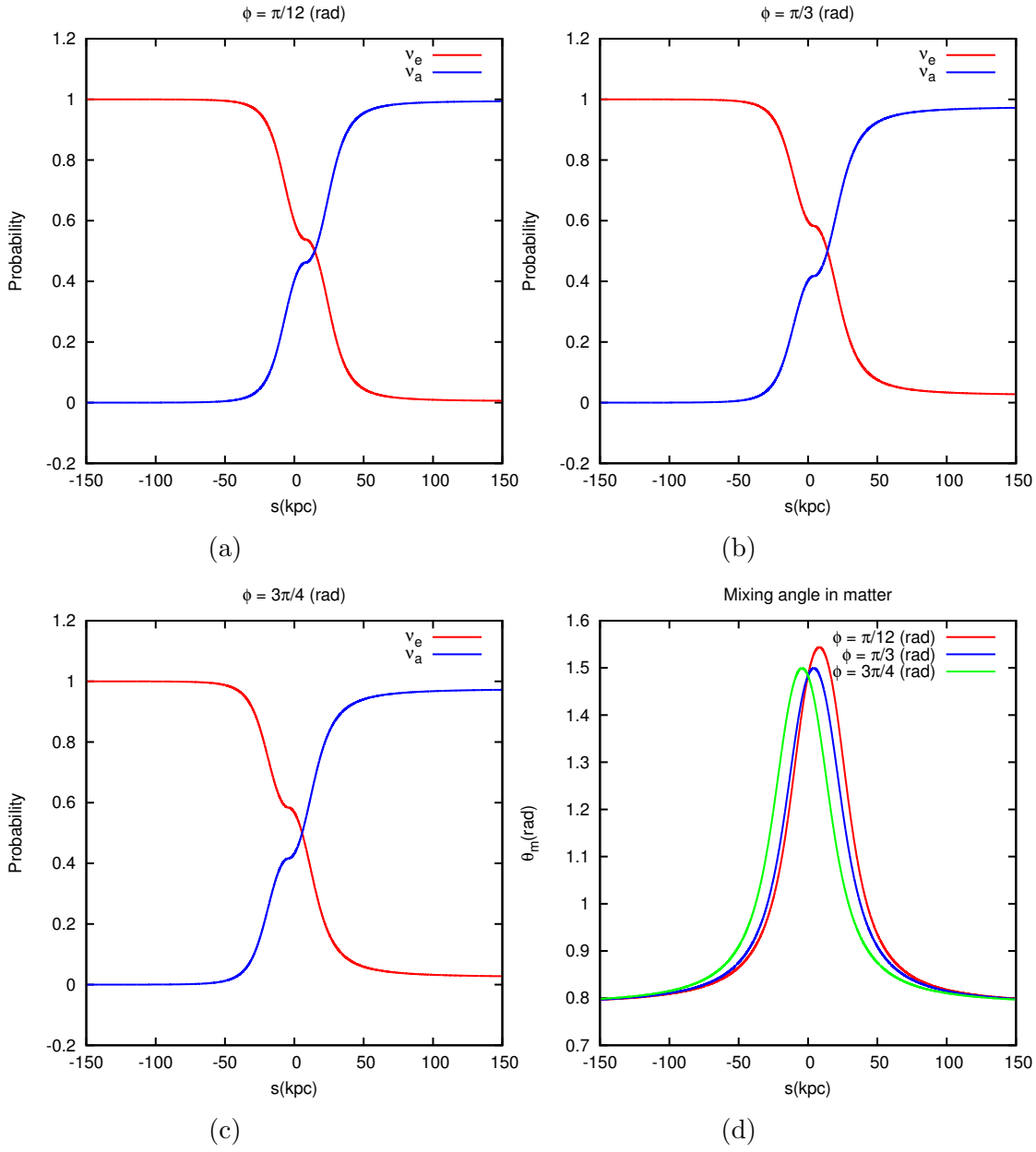

Figure 5.7: Probability of finding an electron neutrino vs non-electron neutrino for V= 10^{-8} GeV^{-1}, θ= 45° and three observation angles ϕ: 15° (top-left), 60° (top-right) and 135° (bottom-left). Comparison of the evolution of the mixing angle in matter in the three cases (bottom-right).

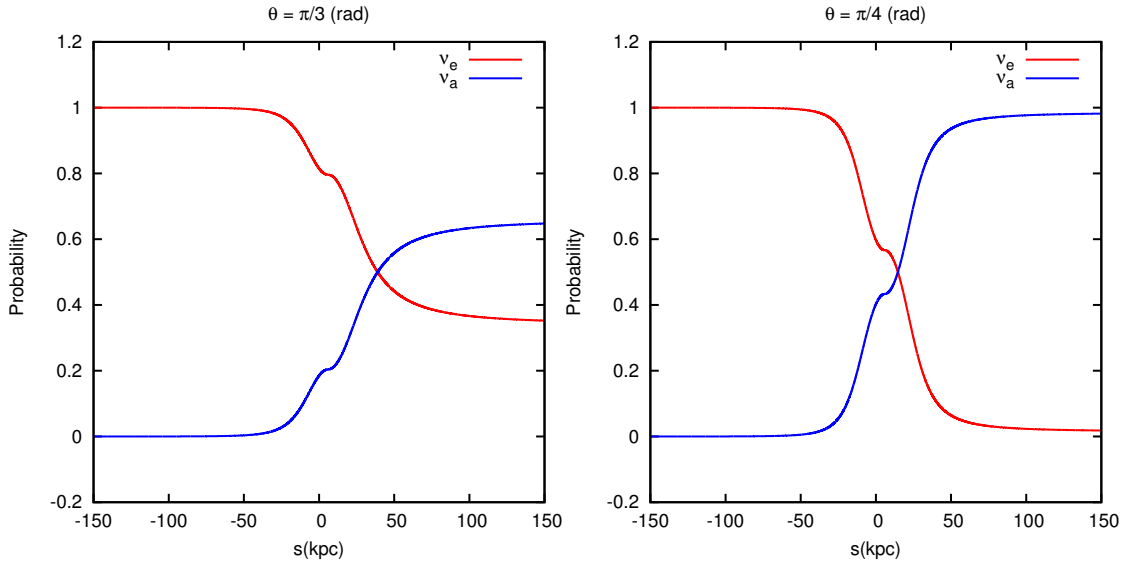

(a) (b)

(c) (d)

Figure 5.8: Probability of finding an electron neutrino vs non-electron neutrino for V= 10^{-8} GeV^{-1}, ϕ= 45° and three vacuum mixing angles θ: 60° (top-left), 45° (top-right) and 15° (bottom-left). Comparison of the evolution of the mixing angle in matter in the three cases (bottom-right).

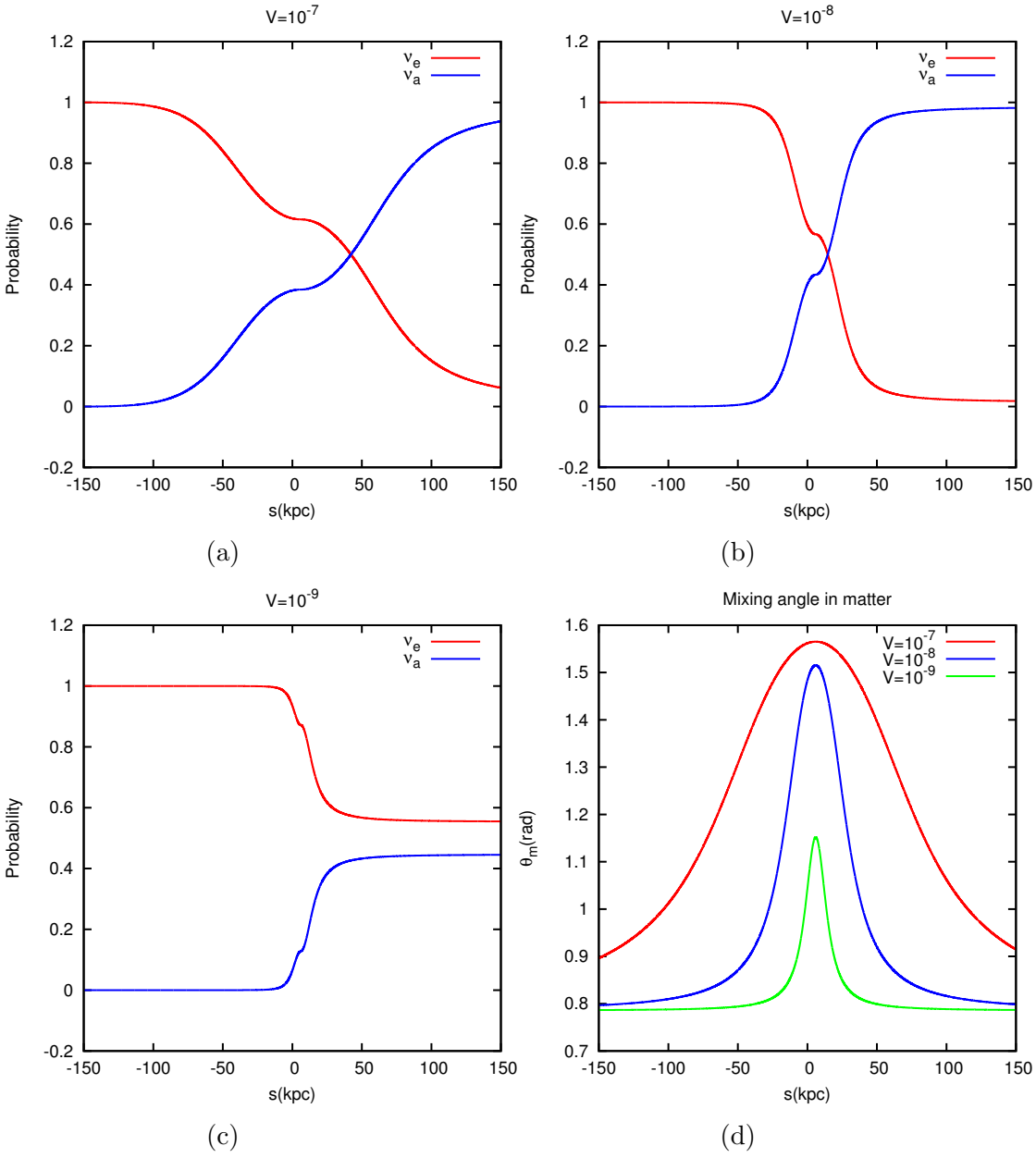

Figure 5.9: Probability of finding an electron neutrino vs non-electron neutrino for ϕ= 45°, θ= 45° and three values of V (in GeV^{-1}): 10^{-7} (top-left), 10^{-8} (top-right) and 10^{-9} (bottom-left). Comparison of the evolution of the mixing angle in matter in the three cases (bottom-right).

Chapter 6

Summary and conclusions

Neutrinos have been presented as weakly interacting particles with very light but non-zero mass whose three flavor eigenstates are mixed and oscillate during propagation. This is an evidence of physics beyond the Standard Model and opens a whole new horizon for investigations in the upcoming years.

The main goal of this thesis was to study the oscillation behaviour of high-energy neutrinos in the cases of vacuum oscillations of three flavors and matter affected oscillations through MSW effect in the two-fflavor approximation. Based on both theoretical concepts and experimental data, we have produced some coherent results that are compatible with current observations and provide interesting options for future lines of investigation. Current data from IceCube is still insufficient to elaborate a statistical comparison with our results for the vacuum model. The future expansion of IceCube will provide a higher rate of events that will allow us to improve the statistical analysis of the track-to-shower ratio, which is the key to study the nature of cosmic sources of neutrinos. Furthermore, the presence of DM in the Universe affects neutrino oscillations and the nature of this obscure component could be better understood through more precise measurements. Our model is sensitive to variations in the potential, which is described by the DM distribution of the Galaxy. Sufficient data could allow us to infer a mass range for the DM particles and establish constraints on the coupling constants to the particles in the SM as well as better models of the spatial distribution throughout the Galaxy.

Further development of this work could be an expansion of the DM model to the three-flavor eigenstates and apply the same procedure as for vacuum oscillations. Then we could analyse the track-to-shower ratio under the effect of a galactic DM halo. This could show new physics based on weak interactions outside the SM.

Bibliography

[1] T. R. S. A. of Sciences. *The Nobel Prize in Physics 2015.* 2015. URL: http://www.nobelprize.org/nobel_prizes/physics/laureates/2015/advanced-physicsprize2015.pdf.

[2] D. Griffiths. "Introduction to Particle Physics". In: *J. Wiley & Sons, Inc* (2014).

[3] W. Pauli. "Letter to the physical society of tubingen". In: *Reproduced in [2]* (1930).

[4] J. Chadwick. "Possible existence of a neutron". In: *Nature* 129.3252 (1932), p. 312.

[5] E. Fermi. "Tentativo di una teoria dei raggi β". In: *Il Nuovo Cimento (1924-1942)* 11.1 (1934), pp. 1–19.

[6] R Brown et al. "Observations with electron-sensitive plates exposed to cosmic radiation". In: *Nature* 163.47-51 (1949), pp. 82–87.

[7] C. F. Powell, D. H. Perkins, and P. H. Fowler. "The study of elementary particles by the photographic method". In: (1959).

[8] C. Cowan Jr and F Reines. "Science 124 103". In: *Phys. Rev* 117 (1956), p. 159.

[9] R. Davis and D. S. Harmer. "Attempt to Observe the Cl37 (ν, e-) Ar37 Reaction Induced by Reactor Antineutrinos". In: *Bull. Am. Phys. Soc* 4 (1959), p. 217.

[10] E. Konopinski and H. Mahmoud. "The universal Fermi interaction". In: *Physical Review* 92.4 (1953), p. 1045.

[11] G. Danby et al. "Observation of high-energy neutrino reactions and the existence of two kinds of neutrinos". In: *Physical Review Letters* 9.1 (1962), p. 36.

[12] M. L. Perl. "The discovery of the tau lepton". In: *History of Original Ideas and Basic Discoveries in Particle Physics*. Springer, 1996, pp. 277–302.

[13] M. Perl. *Searches for Heavy Leptons and Anomalous Past and the Future. SLAC-PUB-1062 (1972), (unpublished).* Tech. rep. 1972.

[14] A. Boyarski et al. "An Experimental Survey of Positron-Electron Annihilation into Multiparticle Final States in the Center of Mass Energy Range 2 GeV to 5 GeV". In: *SLAC Proposal SP-2,(I971)* (1971).

[15] M. L. Perl et al. "Evidence for anomalous lepton production in e+- e- annihilation". In: *Physical Review Letters* 35.22 (1975), p. 1489.

[16] K. Hirata et al. "Observation of a small atmospheric v μ/v e ratio in Kamiokande". In: *Physics Letters B* 280.1 (1992), pp. 146–152.

[17] K. Eguchi et al. "First results from KamLAND: evidence for reactor antineutrino disappearance". In: *Physical Review Letters* 90.2 (2003), p. 021802.

[18] J. Heise. "The Sanford Underground Research Facility at Homestake". In: *Journal of Physics: Conference Series*. Vol. 606. 1. IOP Publishing. 2015, p. 012015.

[19] S Fukuda et al. “Solar B 8 and hep Neutrino Measurements from 1258 Days of Super-Kamiokande Data”. In: *Physical Review Letters* 86.25 (2001), p. 5651.

[20] B. Pontecorvo. “Mesonium and antimesonium”. In: *Soviet Phys. JETP* 6 (1958).

[21] V Gribov and B Pontecorvo. “Neutrino astronomy and lepton charge”. In: *Physics Letters B* 28.7 (1969), pp. 493–496.

[22] Q. Ahmad et al. “Measurement of the Rate of ν e+ d p+ p+ e- Interactions Produced by B 8 Solar Neutrinos at the Sudbury Neutrino Observatory”. In: *Physical Review Letters* 87.7 (2001), p. 071301.

[23] Q. Ahmad et al. “Direct evidence for neutrino flavor transformation from neutral-current interactions in the Sudbury Neutrino Observatory”. In: *Physical Review Letters* 89.1 (2002), p. 011301.

[24] R. Cahn et al. “White paper: measuring the neutrino mass hierarchy”. In: *arXiv preprint arXiv:1307.5487* (2013).

[25] M. Gonzalez-Garcia, M. Maltoni, J. Salvado, and T. Schwetz. “Global fit to three neutrino mixing: critical look at present precision”. In: *Journal of High Energy Physics* 2012.12 (2012), pp. 1–24.

[26] L. Wolfenstein. “Neutrino oscillations in matter”. In: *Physical Review D* 17.9 (1978), p. 2369.

[27] A. Y. Smirnov. “The MSW effect and solar neutrinos”. In: *arXiv preprint hep-ph/0305106* (2003).

[28] S. Mikheyev and A. Y. Smirnov. “Resonant amplification of ν oscillations in matter and solar-neutrino spectroscopy”. In: *Il Nuovo Cimento C* 9.1 (1986), pp. 17–26.

[29] M. Kachelrieß. *Lecture Notes on Quantum Field Theory.* 2015. URL: `http://web.phys.ntnu.no/~mika/cpp7.15.pdf`.

[30] A. Zee. *Quantum field theory in a nutshell*. Princeton university press, 2010.

[31] K. A. Olive et al. *Particle physics booklet*. Review of Particle Physics, Chin. Phys. C38 (2014) 090001, 2014.

[32] F. Hasert et al. “Search for elastic muon-neutrino electron scattering”. In: *Physics letters B* 46.1 (1973), pp. 121–124.

[33] S. L. Glashow and M. Gell-Mann. “Gauge theories of vector particles”. In: *Annals of Physics* 15.3 (1961), pp. 437–460.

[34] S. Weinberg. “A model of leptons”. In: *Physical review letters* 19.21 (1967), p. 1264.

[35] A. Salam and N Svartholm. “Elementary particle theory”. In: *Almquist and Wiksell, Stockholm* (1968), p. 367.

[36] M Kachelriess. “Lecture notes on high energy cosmic rays”. In: *arXiv preprint arXiv:0801.4376* (2008).

[37] C. R. Kitchin. *Astrophysical techniques*. Taylor & Francis, 2013.

[38] P. A. Cherenkov. “Visible emission of clean liquids by action of γ radiation”. In: *Doklady Akademii Nauk SSSR* 2 (1934), p. 451.

[39] S. H. Faria, I. Weikusat, and N. Azuma. “The microstructure of polar ice. Part I: Highlights from ice core research”. In: *Journal of Structural Geology* 61 (2014), pp. 2–20.

[40] V. Y. Lipenkov, N. Barkov, P Dural, and P Pimenta. "Crystalline texture of the 2083 m ice core at Vostok Station, Antarctica". In: *J. Glaciol* 35 (1989).

[41] D. Chirkin. "Evidence of optical anisotropy of the South Pole ice". In: *33 rd International Cosmic Ray Conference, The Astroparticle Physics Conference*. 2013.

[42] A. Delbart, J. Derré, and R. Chipaux. "Cherenkov Radiation Emission in uniaxial optical materials". In: *The European Physical Journal D-Atomic, Molecular, Optical and Plasma Physics* 1.2 (1998), pp. 109–116.

[43] R. E. Mikkelsen and U. I. Uggerhøj. "Characteristics of Cherenkov Radiation in Naturally Occuring Ice". In: *Physical Review D (particles, Fields, Gravitation and Cosmology)* (2015).

[44] U. of Wisconsin-Madison. *IceCube. South Pole Neutrino Observatory*. 2015. URL: `https://icecube.wisc.edu/gallery/press/view/1964`.

[45] IceCube Collaboration, M.G. Aartsen et al. "Evidence for high-energy extraterrestrial neutrinos at the IceCube detector". In: *Science* 342.6161 (2013), p. 1242856.

[46] W. H. Press. *Numerical recipes 3rd edition: The art of scientific computing*. Cambridge university press, 2007.

[47] J. G. Learned and S. Pakvasa. "Detecting ν-τ oscillations at PeV energies". In: *Astroparticle Physics* 3.3 (1995), pp. 267–274.

[48] O. Mena, S. Palomares-Ruiz, and A. C. Vincent. "Flavor composition of the high-energy neutrino events in IceCube". In: *Physical review letters* 113.9 (2014), p. 091103.

[49] A. Palladino, G. Pagliaroli, F. Villante, and F. Vissani. "What is the Flavor of the Cosmic Neutrinos Seen by IceCube?" In: *Physical review letters* 114.17 (2015), p. 171101.

[50] U. of Wisconsin-Madison. *IceCube. South Pole Neutrino Observatory*. 2015. URL: `https://icecube.wisc.edu/science/data/HE-nu-2010-2014`.

[51] Planck Collaboration, P. A. R. Ade et al. "Planck 2015 results. XIII. Cosmological parameters". In: *arXiv preprint arXiv:1502.01589* (2015).

[52] M. Lisanti. "Lectures on Dark Matter Physics". In: *arXiv preprint arXiv:1603.03797* (2016).

[53] C. Grupen. *Astroparticle physics*. Springer Science & Business Media, 2005.

[54] F. W. Dyson, A. S. Eddington, and C. Davidson. "A determination of the deflection of light by the sun's gravitational field, from observations made at the total eclipse of May 29, 1919". In: *Philosophical Transactions of the Royal Society of London A: Mathematical, Physical and Engineering Sciences* 220.571-581 (1920), pp. 291–333.

[55] A. Friedland. "Evolution of the neutrino state inside the Sun". In: *Physical Review D* 64.1 (2001), p. 013008.

[56] M. Kachelriess, A. Strumia, R. Tomas, and J. Valle. "SN1987A and the Status of Oscillation Solutions to the Solar Neutrino Problem (including an appendix discussing the NC and day/night data from SNO)". In: *arXiv preprint hep-ph/0108100* (2001).

[57] P. de Salas, R. Lineros, and M Tórtola. "Neutrino propagation in the galactic dark matter halo". In: *arXiv preprint arXiv:1601.05798* (2016).

[58] J. N. Bahcall and R. M. Soneira. “The universe at faint magnitudes. I-Models for the galaxy and the predicted star counts”. In: *The Astrophysical Journal Supplement Series* 44 (1980), pp. 73–110.